Available online at www.sciencedirect.com

SCIENCE DIRECT®

Tectonophysics 407 (2005) 135–163

TECTONOPHYSICS

www.elsevier.com/locate/tecto

Intra-arc transpression in the lower crust and its relationship to magmatism in a Mesozoic magmatic arc

Stephen B. Marcotte [a], Keith A. Klepeis [a,*], Geoffrey L. Clarke [b], George Gehrels [c], Julie A. Hollis [b]

[a] *Department of Geology, University of Vermont, Burlington, VT, 05405-0122, USA*
[b] *School of Geosciences, Division of Geology and Geophysics, University of Sydney, NSW 2006, Australia*
[c] *Department of Geosciences, University of Arizona, Tucson, AZ, 85721, USA*

Received 9 September 2004; received in revised form 4 July 2005; accepted 18 July 2005
Available online 12 September 2005

Abstract

Structural observations and U–Pb geochronology from Fiordland, New Zealand support a model of partitioned transpression within the lower crust of an early Mesozoic magmatic arc called the Median Batholith. We use this lower crustal section to test whether transpression was an efficient mechanism for transporting magma through the deep lithosphere. A continentward migration of magmatic activity occurred within the margin of Gondwana after ~140 Ma followed by a period of concentrated magmatism in a vertical, 12–15 km wide lower crustal shear zone after ~119 Ma. The shear zone, named the Indecision Creek Shear Zone, contains variably oriented dioritic intrusions and displays systematic variations in the three-dimensional orientation of ductile structures. From the margins to the center of the shear zone the pitch of stretching lineations on foliation surfaces changes from 10–35° to 55–82° with increasing finite strain. This increase in pitch is accompanied by a steepening and counter-clockwise rotation of foliation planes. These and other structural patterns indicate that arc-parallel sinistral oblique-slip and strike-slip displacements occurred at the shear zone margins and that deformation in its center was dominated by horizontal arc-normal shortening and near vertical extrusion. This style of partitioned transpression reflects the effects of rheological contrasts created by a heterogeneous pattern of magmatism within the arc. Field relationships and U–Pb dates on zircon suggest that the shear zone formed along the boundary between outboard (older) and inboard (younger) parts of the batholith and facilitated the transfer of small volumes of magma vertically through the lower crust until at least ~111 Ma, when convergence and arc magmatism waned.

Keywords: Oblique convergence; Transpression; Arc magmatism; U–Pb geochronology

* Corresponding author. Tel.: +1 802 656 0247; fax: +1 802 656 0045.
E-mail address: kklepeis@uvm.edu (K.A. Klepeis).

0040-1951/$ - see front matter © 2005 Elsevier B.V. All rights reserved.
doi:10.1016/j.tecto.2005.07.007

1. Introduction

The concept of transpression has helped geoscientists understand and visualize the three-dimensional nature of deformation in the Earth's crust and upper mantle (Dewey et al., 1998; McCaffrey, 1992; Cembrano et al., 2002; Jones et al., 2004). Transpression, as defined here, refers to deformation that is accommodated by simultaneous strike-slip and contractional displacements. At the scale of plate margins, transpression can be strike-slip partitioned where displacements occur on separate strike-slip and contractional structures, such as in the San Andreas fault system (Teyssier and Tikoff, 1998). The deformation also may be relatively homogeneous where strike-slip and contractional displacements occur in the same place or are distributed uniformly across a zone. The Australian–Pacific plate boundary zone in the central part of the South Island of New Zealand is an example of this latter style of transpression (Norris and Cooper, 1995).

Despite its probable widespread occurrence, there are many aspects of transpression which are uncertain. One unresolved issue centers on the factors that control how transpression evolves in an extremely heterogeneous, anisotropic lower crust. Analogue and mathematical models predict that a change from strike-slip-dominated to thrust-dominated transpression occurs at a convergence angle of 20° (e.g., Tikoff and Teyssier, 1994). These models explain the origin of variations in the degree of strike-slip partitioning at obliquely convergent margins and have tended to work well for many upper crustal fault systems. However, authors increasingly have noted that rheological contrasts, including those associated with magmatism, also strongly influence deformation partitioning (Coke et al., 2003; Tavarnelli et al., 2004). This effect has created uncertainty about the characteristics of transpression in the deep crust and how various types of boundary conditions control its evolution. Mathematical models that describe the evolution of structural elements that define ductile transpression for different scenarios have outpaced the description of natural examples.

Another aspect of transpression that is uncertain concerns its relationship to magma transport. At obliquely convergent plate margins where subduction has led to magmatism, deformation typically is accommodated within the magmatic arc because of the high heat flow and rheological contrasts that characterize these provinces. In these settings transpression has been postulated to be an efficient mechanism for transporting magma vertically and horizontally through the lithosphere (Saint Blanquat et al., 1998). Buoyancy forces and the dynamics of transpression may cause an overpressuring of magma, which then may follow a vertical pressure gradient. However, some experiments suggest that local pressure gradients caused by rheological boundaries may inhibit the vertical extrusion of material, especially in the deep crust (Czeck and Hudleston, 2004). Models describing the feedbacks that can develop between magmatism and transpression can be difficult to test directly because structures that may reveal the interplay between magmatism and deformation, such as those which occur in migmatite, are easily destroyed.

In this paper, we use exposures of the lower crust located in northern Fiordland, New Zealand to examine relationships between deformation and magmatism in an early Mesozoic magmatic arc represented by the Median Batholith (Fig. 1; Mortimer et al., 1999a). New data presented here include 1) detailed structural measurements and a kinematic analysis of deformation across a ~20 km wide transect of a steep, lower crustal shear zone recently discovered by Klepeis et al. (2004); 2) a characterization of the sequence of intrusions that occur within and outside the shear zone; 3) and six U–Pb isotopic analyses of zircon from pre-, syn- and post-tectonic dikes. We also report the first age determination from the George Sound Shear Zone. The new data allow us to establish a transpressive style of deformation within the lower crust of this arc and to determine the factors that influenced the partitioning of displacements within it. The results support a model of transpression where triclinic symmetry is achieved by a kinematic partitioning of dip-slip and oblique-slip displacements in three dimensions. The analyses show that transpression resulted from convergence between two terranes that were characterized by different ages and temperatures, and helped move magma through the lower crust after ~119 Ma until at least ~111 Ma. However, the amount of magma transported through the lithosphere by this mechanism probably was minor. The small volume of magma associated with transpression appears to reflect the occurrence of the deformation

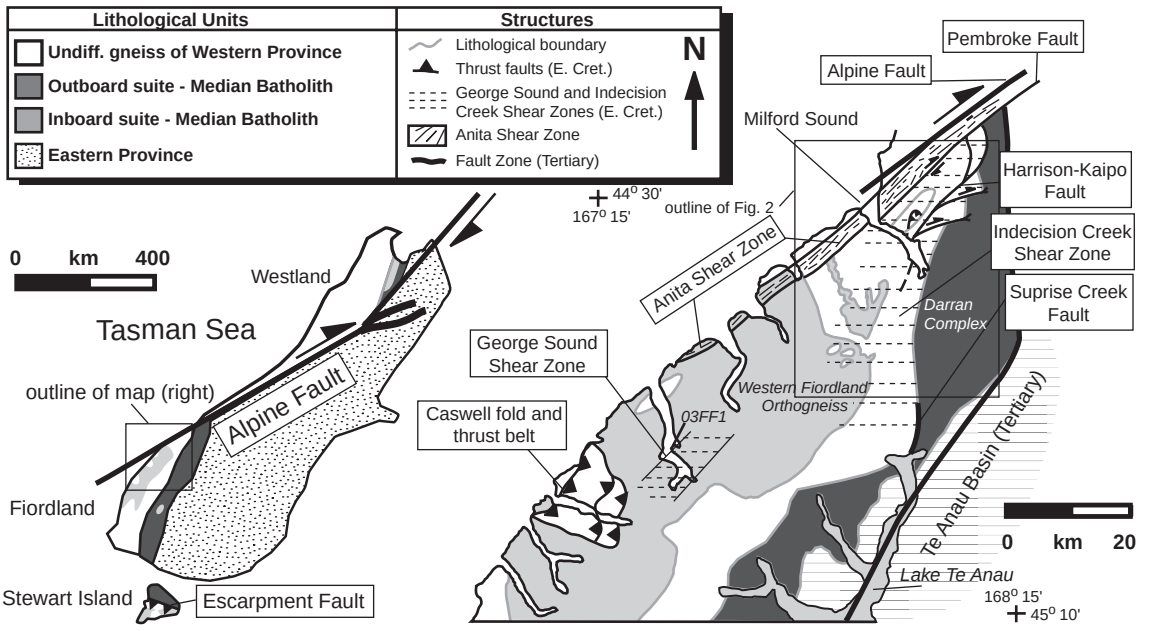

Fig. 1. Simplified geologic map (left) of the South Island, New Zealand after Mortimer et al. (1999a) and Tulloch and Kimbrough (2003). Detailed map of northern Fiordland (right) shows lithological boundaries and major faults. Early Cretaceous contractional structures shown include the George Sound Shear Zone, the Indecision Creek Shear Zone, the Caswell fold and thrust belt, and the Escarpment Fault (after Allibone and Tulloch, 1997) and the Pembroke thrust. Late Tertiary faults, including the Harrison–Kaipo (after Claypool et al., 2002) and the Surprise Creek (after Bradshaw, 1990) faults reactivate the boundary between the Western Province (inboard terrane) and the Eastern Province (outboard terrane) of the Median Batholith.

during the waning stages of arc magmatism after periods of the voluminous magmatism had already ceased. Microstructural data show that the dominant fabrics of the shear zone record are mostly subsolidus conditions, indicating that the deformation outlasted magmatism.

2. Geologic setting

Northern Fiordland records a history of magmatism, high grade metamorphism and convergence that occurred along the margin of Gondwana during early Mesozoic times. The Median Batholith (Fig. 1) was formed as a result of subduction during this period. The batholith is divided into outboard (currently eastern) and inboard (currently western) belts (see Tulloch and Kimbrough, 2003 for a review). The outboard belt was initially constructed close to and offshore of Gondwana during the early Mesozoic, with a volumetrically dominant period of igneous activity occurring during the interval 168–137 Ma (J.D. Bradshaw, 1993; Kimbrough et al., 1993, 1994; Muir et al., 1998; Nathan et al., 2000). Subsequently, the outboard belt accreted onto the Gondwana margin. Hollis et al. (2003) suggested that the amalgamation occurred as early as ~136 Ma and probably before ~129 Ma. Continued igneous activity resulted in the emplacement of the inboard magmatic belt during the period ~129–105 Ma (Muir et al., 1995; Tulloch and Kimbrough, 2003; Hollis et al., 2003).

In northern Fiordland (Figs. 1 and 2) continental margin assemblages are represented by the St. Anne and Thurso gneisses and undifferentiated metasedimentary and plutonic rock of Paleozoic age. The Darran Complex (Koons, 1978; Wandres et al., 1998; Blattner and Graham, 2000) represents the outboard belt and the Western Fiordland Orthogneiss (Bradshaw, 1989a,b) represents part of the inboard belt of the Median Batholith. The former belt is composed of mostly unmetamorphosed gabbroic, dioritic and granitic rocks that were emplaced into the upper crust. The latter belt is composed of metagabbroic and metadioritic layers that contain high-

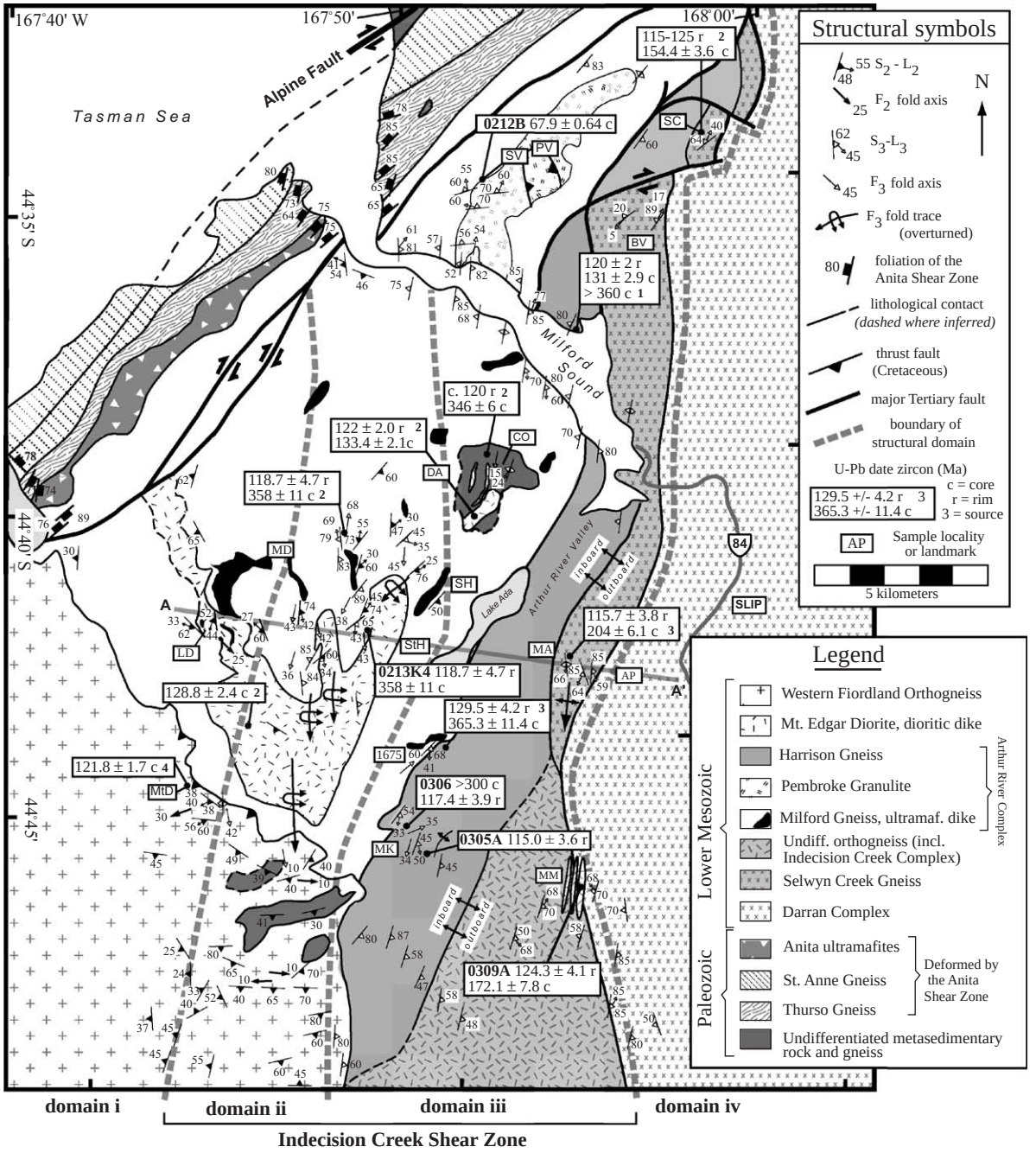

Fig. 2. Structural map of the Milford Sound region showing major lithological divisions and field stations. U–Pb dates on zircon are from this paper (sample numbers provided, r—rim age, c—core age) and the following published sources: (1) Tulloch et al. (2000), (2) Hollis et al. (2003), (3) Klepeis et al. (2004), (4) Hollis et al. (2004). Structural data are from this study and the following sources: Wood (1962), Blattner (1976), Klepeis et al. (1999), Daczko et al. (2001a,b), Turnbull (2000) and Klepeis et al. (2004). Measurements south of MtD, MK and MM are from Bradshaw (1990). DA, Devil's Armchair; SV, Stirling Valley; PV, Pembroke Valley; BV, Bowen Valley; SC, Selwyn Creek; CO, Camp Oven Creek; MA, Mt. Ada; AP, Access Peak; SLIP, Slip Creek on the Milford Road; 1675, Peak 1675; SH, Shoulder Hill; StH, Steep Hill; MD, Mt. Danger; LD, cirque northwest of Lady of the Snows; MtD, north slope of peak 1482, southeast of Mt. Daniel; MK, ridge and saddle southeast of Mt. Kepka. Profile A–A′ is shown in Fig. 3.

pressure (12–14 kbar) upper amphibolite and granulite facies mineral assemblages indicative of metamorphism at lower crustal depths of ~45 km (Bradshaw, 1989a,b; Daczko et al., 2002b; Clarke et al., 2005). Between these two units are a series of high grade, locally migmatitic gneisses that comprise the Arthur River Complex. This latter unit displays affinities to both the inboard and outboard belts (Hollis et al., 2003) and has been subdivided into the mostly gabbroic Milford Gneiss (Wood, 1962, 1972; Blattner, 1978, 1991), the mostly dioritic Harrison Gneiss (Blattner, 1978, 1991), and the Pembroke Granulite (Blattner, 1991; Daczko et al., 2001a). Klepeis et al. (2004) suggested that a belt of high grade rocks called the Selwyn Creek Gneiss (Fig. 2) represents the deformed western margin of the Darran Complex. South of Milford Sound, the dioritic Indecision Creek Complex of Bradshaw (1990) separates the Darran Complex from the Western Fiordland Orthogneiss and grades into the Harrison and Selwyn Creek gneisses.

Relationships at Mt. Daniel (MtD, Fig. 2) indicate that the Western Fiordland Orthogneiss intrudes the Milford Gneiss (Bradshaw, 1990). Published ages from the former unit range from ~126 to ~116 Ma (Mattinson et al., 1986; Muir et al., 1998; Tulloch and Kimbrough, 2003; Hollis et al., 2004). Tulloch and Kimbrough (2003) and Hollis et al. (2004) report high precision U–Pb dates on zircon suggesting the main phase of the unit was emplaced during the interval 126–120 Ma. Hollis et al. (2003) dated a 128.8 ± 2.4 Ma body structurally below the Western Fiordland Orthogneiss, which we name the Mt. Edgar Diorite (Fig. 2).

An up-pressure metamorphic history for the Western Fiordland Orthogneiss and the Arthur River Complex was first proposed by Bradshaw (1989a,b, 1990) and Bradshaw and Kimbrough (1989) using metamorphic *P–T* paths. Clarke et al. (2000) confirmed burial from $P<8$ to 12–14 kbar for the Arthur River Complex on the basis of changes in metamorphic mineral assemblages. Oliver (1990) and Brown (1996) suggested that the burial reflected magma loading caused by the emplacement of the Western Fiordland Orthogneiss. Daczko et al. (2002c) suggested that thrust faulting in the mid-crustal Caswell fold and thrust belt (Fig. 2) played an important role in the burial of these units. Klepeis et al. (2004) showed that lower crustal thickening was accomplished by displacements on both steep and gently dipping shear zones. These shear zones (Figs. 1 and 2) include the Pembroke thrust (Daczko et al., 2001b), and the Indecision Creek and George Sound shear zones (Klepeis et al., 2004).

3. Structural geology

Four structural domains (Figs. 2 and 3) are distinguished on the basis of structural style, and the orientation of rock fabrics and their relative time of formation. From west to east (Fig. 2), these domains are the following: (i) domain of igneous layering, (ii) domain of polyphase folding, (iii) domain of tight folds and shear zones and (iv) the eastern domain. The domains are defined independently of lithology, although their boundaries tend to follow lithologic contacts.

3.1. Domain i: domain of layered igneous intrusions

The Mt. Edgar Diorite and Western Fiordland Orthogneiss are composed of gneissic and igneous layering that dips moderately to the south and southwest (Fig. 4a,b). Individual layers of diorite, gabbro and lesser ultramafic rock range in thickness from tens to hundreds of meters. The oldest foliations in this domain (collectively referred to here as S_1) are preserved in pods or boudins of gabbroic gneiss (Fig. 4d). These pods are enveloped by a penetrative foliation (S_2) that dips to the south and southwest (Fig. 4c). This foliation is defined by flattened clusters of plagioclase, quartz, biotite, hornblende and garnet. The S_2 foliation approximately parallels the lower contacts of the Western Fiordland Orthogneiss and the Mt. Edgar Diorite (Fig. 4b) and forms the dominant structure of this domain. Recumbent, isoclinal folds (F_2) of S_1 display axial planes that parallel S_2 foliation planes (Fig. 4d). F_2 fold axes plunge to the southwest and southeast. A mineral lineation (L_2) defined by aligned hornblende, clinozoisite, plagioclase and biotite plunges variably to the northwest and southeast on S_2 surfaces (Fig. 4c).

3.2. Domain ii: domain of polyphase folding

Domain ii is defined by a zone of polyphase folding in the Arthur River Complex (Fig. 2, StH, MD,

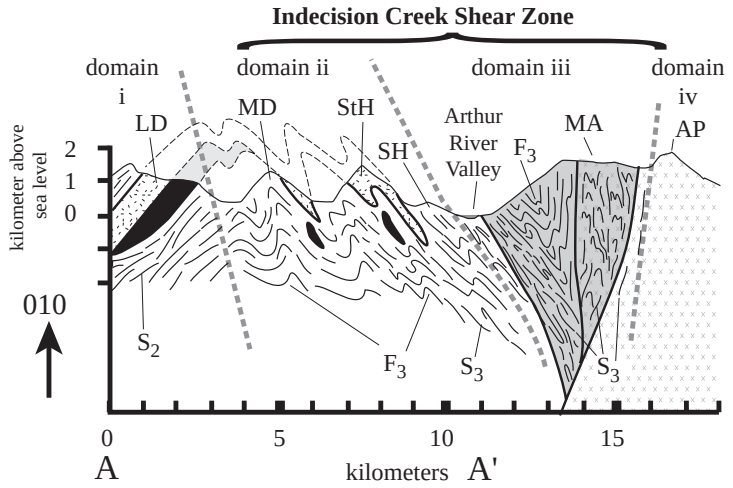

Fig. 3. Profile (A–A′) illustrating the structure of domains i, ii, iii and iv. Explanation of rock units, abbreviations and profile location are in Fig. 2. Domain boundaries are shown with dashed lines. See text for explanation.

SH) and the Western Fiordland Orthogneiss (Fig. 2, MtD). The oldest foliations (S_1) are locally preserved as gneissic layering that is cut by mafic and dioritic dikes. In most places these foliations and dikes are transposed parallel to a penetrative gneissic foliation (S_2) that it identical in composition and orientation to the S_2 foliation in domain i. Recumbent, isoclinal folds (F_2) of mafic dikes are intrafolial and display axial planes that parallel S_2 surfaces, which mostly dip to the south and southwest. A mineral lineation (L_2) defined by aligned plagioclase, biotite and hornblende plunges variably to the north , south and southwest on S_2 surfaces. Garnet–plagioclase–quartz leucosome in migmatitic gneiss parallels the S_2 foliation.

The S_2–L_2 fabric is folded (F_3, Fig. 5a,b) into a series of upright, northwest-verging folds that plunge ~30° to the south (Fig. 5c). These upright folds dominate the structure of domain ii. Crenulation cleavage planes (S_3) that approximately parallel the axial planes of F_3 folds (Fig. 5b) dip steeply to moderately to the south, east and southeast (Fig. 5d). A mineral lineation (L_3) defined by aligned clusters of plagioclase, amphibole, and garnet plunges ~30° to the south on S_3 surfaces parallel to F_3 fold axes (Fig. 5d).

3.3. Domain iii: domain of tight folds and shear zones

Throughout domain iii, elongate pods of gabbro and older paragneiss are surrounded by younger dioritic intrusive rock. Like elsewhere, these pods preserve the oldest structures of the domain. Near Mt. Kepka (MK, Fig. 2), the transitional contact between the gabbroic Milford Gneiss and the dioritic Harrison Gneiss is well exposed. In this area, rocks of the Harrison Gneiss intrude those of the Milford Gneiss, indicating that the former unit is younger than the latter (Fig. 6a and b).

We refer to the oldest groups of foliations preserved in pods of gneiss as S_1. These foliations display a weak to moderate alignment of medium to coarse plagioclase, hornblende and clinozoisite, which is interpreted here as recrystallized igneous layering. Inside the pods, S_1 surfaces and dikes are folded into tight-isoclinal folds (F_2) that display an axial planar foliation (S_2). The S_2 foliation is defined by flattened, stretched and aligned plagioclase, hornblende and clinozoisite. S_2 surfaces are refolded by tight to isoclinal folds (F_3) that plunge moderately and steeply to the south. A penetrative subvertical foliation (S_3) parallels the axial planes of the F_3 folds and is especially well developed along the highly attenuated limbs of these folds (Fig. 6c). The S_3 foliation dips variably to the east and southeast and displays a penetrative down-dip hornblende, biotite and plagioclase mineral lineation (L_3) that plunges variably to the south and southwest (Fig. 6d and e). These steep foliations form a discontinuous pattern of high strain zones (Fig. 6c).

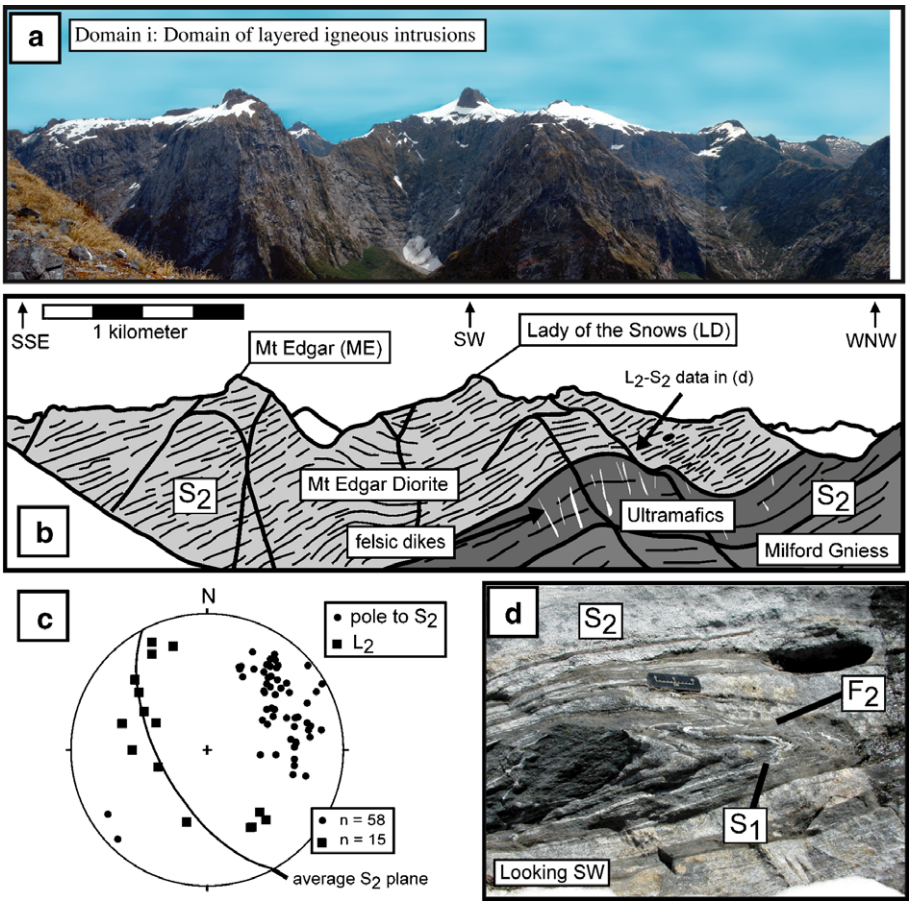

Fig. 4. Panoramic photograph (a) and sketch (b) of the Mt. Edgar Diorite as viewed from Mt. Danger (MD, Fig. 2). Sketch shows the contact between the Mt. Edgar Diorite and the older Milford Gneiss. The margins of the intrusion parallel compositional layering (S_2) in host rock. From left to right, S_2 orthogneiss layering in the Milford Gneiss and Mt. Edgar Diorite is folded into a broad F_3 synform. Vertical dikes (white, b) cut the ultramafic bodies at high angle to S_2. LD is Lady of the Snows (Fig. 2). (c) Lower hemisphere, equal area stereoplot of S_2 and L_2 from the Mt. Edgar Diorite and Western Fiordland Orthogneiss. (d) Recumbent, isoclinal F_2 enveloped by S_2 foliation.

There is abundant evidence for minor shear zone development and syntectonic dike emplacement throughout domain iii. Felsic pegmatites and dioritic dikes that cut S_3 are variably folded by F_3 folds (Fig. 6c and f), indicating that they were emplaced during the deformation that produced the F_3 folds and S_3 foliations. Cross cutting relationships and variations in the degree of F_3 folding allow a sequence of dike emplacement to be determined. Older dikes are isoclinally folded or have been stretched into boudins that parallel the S_3 foliation (Fig. 7a). Some of these boudins are asymmetric and display sinistral displacements at high angles to L_3 on horizontal surfaces (Fig. 7b and c). Younger dikes cut S_3 foliation planes or are weakly foliated and display tight to open F_3 folds (Fig. 6f).

This history of syntectonic magmatism produced a vertically layered igneous fabric that parallels the S_3 foliation (Fig. 7a). Rheological differences among these layers influenced the partitioning of strain within this domain. Dikes in fine-grained mafic layers record more shortening than in adjacent coarse-grained felsic layers. This is illustrated by the variations in fold tightness in a single felsic dike shown in Fig. 7a (arrows). The effect is most likely due to differences in grain size where fine-grained layers are weaker than coarse-grained layers. According to Passchier and Trouw (1996)

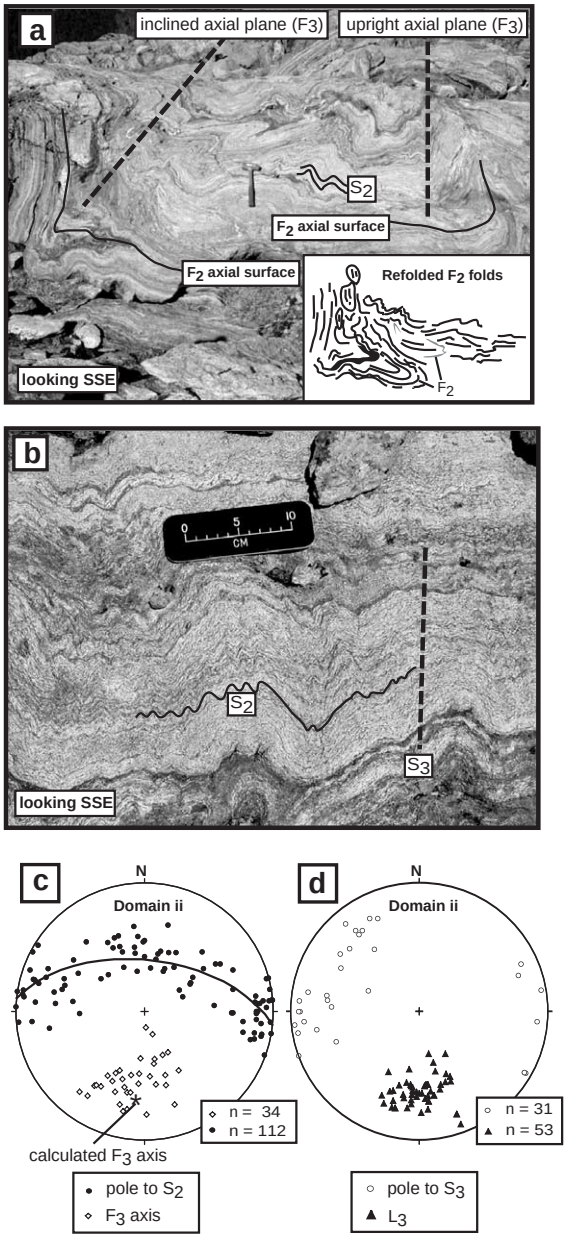

Fig. 5. Structural data from domain ii. (a) Tight and open parasitic F_3 folds (StH, Fig. 2) that are part of an overturned F_3 fold. Hammer in center is 12 in. tall. (b) Open F_3 folds and S_3 crenulations in the Milford Gneiss from near the lower contact of the Western Fiordland Orthogneiss (MtD, Fig. 2). Biotite is bent within S_3 crenulations. (c) Lower hemisphere, equal area stereoplot of folded S_2 foliation surfaces and south-plunging F_3 fold axes in domain ii. (d) Lower hemisphere, equal area stereoplot of the steeply dipping S_3 foliation and plunging L_3 mineral lineations in domain ii. Both stereoplots (c and d) show data from Steep Hill and Mt. Danger (Fig. 2, StH and MD).

these rheological differences may reflect the dependence of strain rate on grain size in cases where solid-state diffusion is an important deformation mechanism.

3.4. Domain iv: eastern domain

Domain iv contains plutonic rock of the Darran Complex and the Selwyn Creek Gneiss. This latter unit represents the deformed western margin of the Darran Complex. Mt. Mitchelson (MM, Fig. 2), which lies along the boundary between these two units, lacks the penetrative ductile fabrics that dominate domain iii. Instead, the deformation is localized along the margins of dioritic and gabbroic dikes. In a coarse-grained gabbroic host, a weak foliation dips steeply to the west–northwest (Fig. 8a, bottom left). On foliation planes weakly aligned aggregates of hornblende and plagioclase define a mineral lineation that plunges ~70° to the northwest. Fine-grained gabbroic and dioritic dikes cut across this foliation at high angles, displaying both sharp and undulate contacts with the coarse-grained gabbroic host. These structures are interpreted to be similar to those that may have characterized domain iii prior to intense deformation.

The dominant structural feature at Mt. Mitchelson is a series of subvertical dioritic dikes that intrude a coarse-grained, weakly foliated gabbroic host. These dikes exhibit contacts that parallel the overall trend of the Median Batholith. The dikes display 15 m wide brecciated zones (Fig. 8b) at there margins where angular clasts of gabbroic host rock are surrounded by unfoliated, biotite-bearing diorite. Clasts of the host rock contain folds of foliation that are not observed in the adjacent wall rock (Fig. 8b, center). Veins of the diorite fill fractures displaying tapered tips and straight boundaries (Fig. 8b), suggesting that high strain rates and melt-enhanced fracturing produced the brecciated zone during dike emplacement. Where these veins cut the fine gabbro and diorite dikes they are openly folded and display axial planes that parallel the dike margins. These observations suggest that deformation during or following dike emplacement was focused within the younger dikes rather than in the coarse-grained gabbro host. The occurrence of the brecciated zones and lack of chilled margins suggests rapid emplacement of the

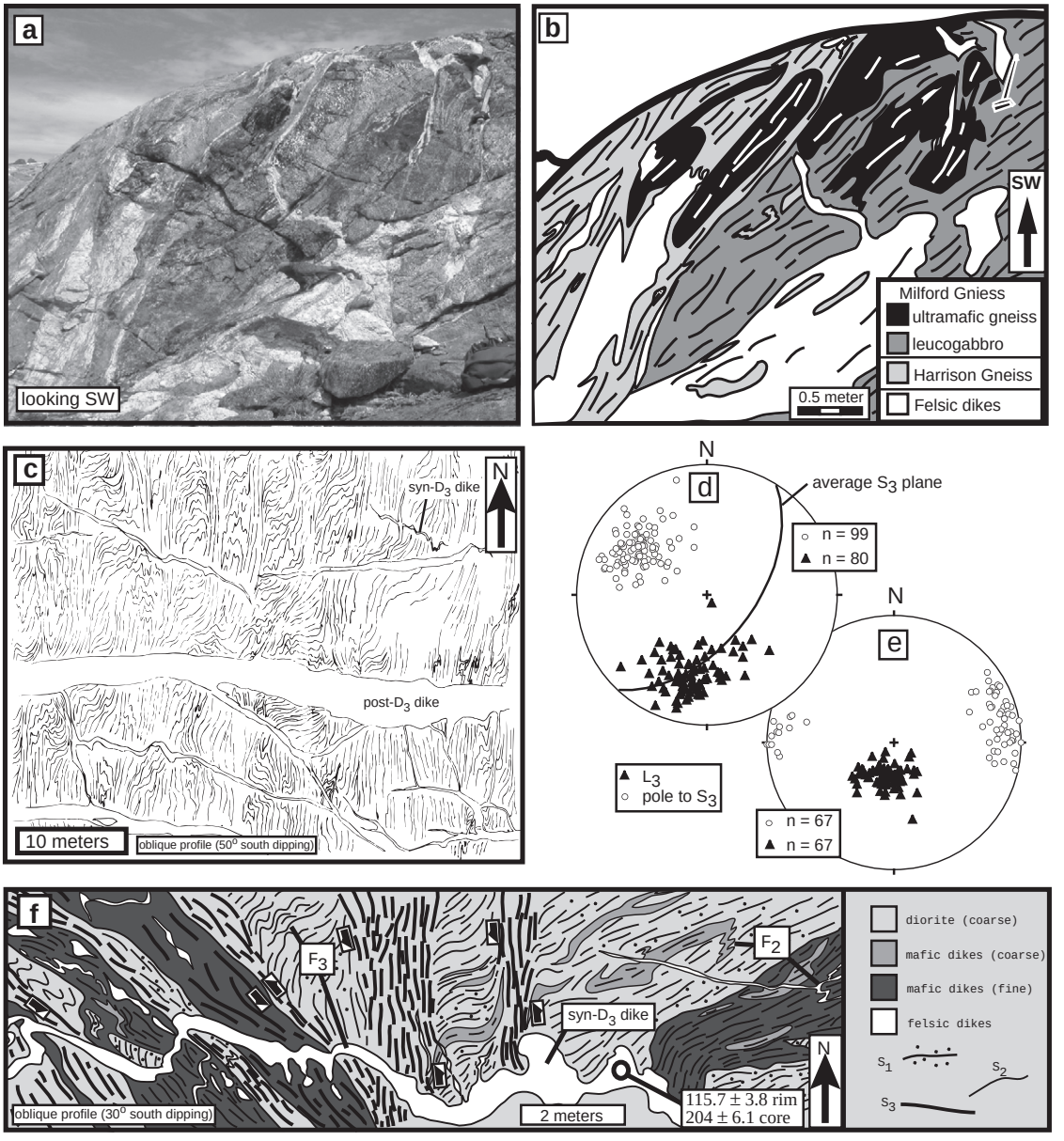

Fig. 6. Photograph (a) and interpretive sketch (b) showing the intrusive relationship between a dioritic dike of the Harrison Gneiss (left) and gabbroic and ultramafic gneiss of the Milford Gneiss (right) exposed southeast of Mt. Kepka (MK, Fig. 2). Note that the igneous layering (S_1) in the gabbroic and ultramafic pod is cut by the younger dioritic intrusive rock, which contains the S_3 foliation. (c) 50 ± 50 m sketch showing the heterogeneous, domainal nature of fabric preservation in the Indecision Creek Shear Zone at Mount Ada (MA, Fig. 2). Mapped surface dips 30° to the south (bottom of map). Note the presence of syntectonic (folded) dikes. (d and e) Lower hemisphere, equal area stereoplots of S_3 foliation planes and L_3 mineral lineations from Mt. Kepka in the Harrison and Milford gneisses (a and b) and from Mt. Ada in the Selywn Creek Gneiss (c). (f) Map of a surface that is slightly tilted to the north showing the relationships among dikes and shear zone foliations (S_3) in the Indecision Creek Shear Zone at Mt. Ada. Note asymmetric foliation showing a component of arc-parallel (north-trending) sinistral displacement at high angles to a steeply south-plunging L_3 mineral lineation. A minor dextral component of displacement on surfaces that strike to the northwest also occurs within the outcrop. Syntectonic dikes were emplaced during the deformation that produced the shear zone and the F_3 folds. U–Pb ages on zircon from sample Ada2 of Klepeis et al. (2004) is shown.

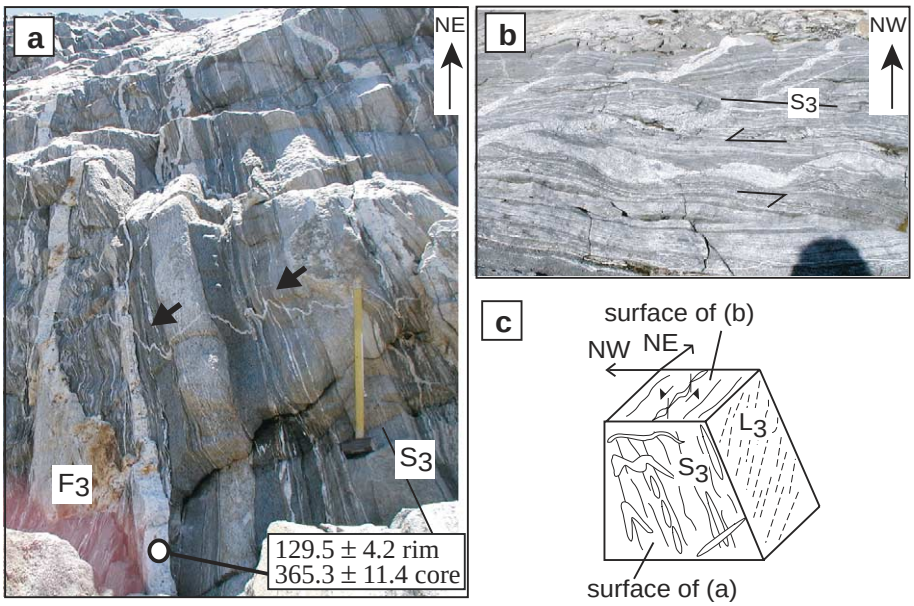

Fig. 7. (a) Photograph showing multiple generations of variably folded dioritic and felsic dikes that intruded the Indecision Creek Shear Zone in the Harrison Gneiss. U–Pb ages on zircon from sample 0221K of Klepeis et al. (2004) is shown. The arrows point to a folded felsic dike that displays heterogeneous shortening within different lithological units that define the S_3 foliation. (b) Photograph of a sub-horizontal pavement that displays asymmetric boudinage of a dioritic dike. Sense of shear is sinistral. (c) Block diagram showing the geometry of S_3 and L_3 structures and the occurrence of sense of shear indicators at a high angle to a steeply plunging mineral stretching lineation (L_3).

dioritic dikes into a crystallized, but still hot gabbroic host.

4. Definition of the indecision creek shear zone

In this section we correlate S_3, L_3 and F_3 structures in domains ii and iii and use variations in their geometry to define gradients in finite strain and to locate the boundaries of the Indecision Creek Shear Zone. The correlations are based on the following relationships: 1) S_3, L_3 and F_3 always appear together, 2) these structures display similar sequences of formation relative to other structures in the two domains, 3) rim ages on zircon from syntectonic dikes in both domains (Fig. 11 and Section 7 of this paper) indicate that these structures formed during the same time interval (after ~119 Ma until at least ~111 Ma). Table 1 summarizes our correlations and those in previously published papers.

Variations in the interlimb angles of mesoscale F_3 folds define a linear increase in D_3 finite strain from west to east across domains ii and iii, which we used to locate the shear zone's western boundary. Measurement localities included MD, StH, MtD, CO, MA (Fig. 2). The interlimb angles are variable (Fig. 9a), reflecting the heterogeneous geometry of the F_3 folds. Domain ii displays a wide range (30–120°) of angles with an average of ~43°. Domain iii shows a narrow range of angles, with most between 5° and 42°, and an average of ~22°. This latter measure is an over estimate because it does not include the transposed folds that occur in high strain zones. The results suggest that a component of shortening normal to the shear zone increases from at least 30–40% in domain ii to >60% shortening in domain iii. The boundary between domains ii and iii (Fig. 2) is located where F_3 folds first appear transposed and the S_3 foliation is dominant along a west to east transect.

As the F_3 folds tighten across domain ii, S_3 foliation planes steepen (Fig. 9d and e) and S_2 is transposed parallel to S_3 in locally mylonitic shear zones. The transposition of S_2 also is accompanied by a change in the average orientation of gabbroic and dioritic dikes from parallel to S_2 in domain i to

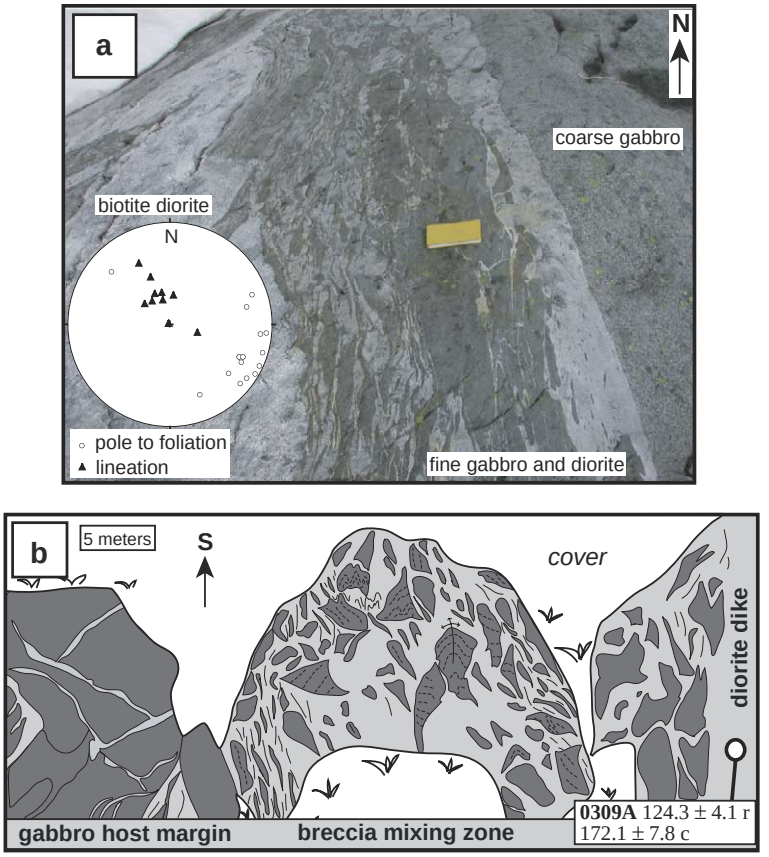

Fig. 8. Structure of domain iv at Mt. Mitchelson. (a) Photograph showing at least four phases of intrusive rock. The oldest intrusion is a coarse-grained gabbro (right) that is cut by dikes of fine-grained gabbro and diorite (center). Elongate clasts of fine-grained gabbro enveloped by the younger diorite parallel the dike margins. These dikes are cut by a biotite-bearing dioritic dike (left). The margins preserve evidence of ductile deformation including folding and rotation of gabbroic clasts. Lower hemisphere, equal area stereoplot (bottom left, a) shows poles to foliation and a mineral lineation defined by hornblende and plagioclase in coarse-grained gabbro. (b) Outcrop sketch of the brecciated margin of a dioritic dike that is 50 m wide (MM , Fig. 2.). Sample 0309A (Fig. 11q) is from the xenolith free interior of the dike show in b.

parallel to S_3 in domains ii and iii. These patterns reflect the increase in D_3 finite strain from west to east across a 3–5 km wide zone in domain ii. A similar change in finite strain occurs from east to west from domain iv into domain iii near Selwyn Creek (SC, Fig. 2). This latter gradient is very narrow (<1 km) and difficult to access due to the mountainous terrain. Measurements indicate that both the eastern and western boundaries of the Indecision Creek Shear Zone are nearly vertical and

Table 1
Correlation of deformation events in N. Fiordland with published interpretations

This study	Hollis et al. (2004)	Klepeis et al. (2004)	Daczko et al. (2001a,b), Hollis et al. (2003)	Wandres et al. (1998)	Bradshaw (1990)	Blattner (1978)
D_1		D_1	D_1	l_1, l_2	D_1, WFO	
D_2	D_1MD, D_1 GS	D_2	D_2, GRZ	D_1, 1_3	D_2, WFO	D_{n-2}, GRZ
D_3	D_2MD, D_2 GS	D_3	D_3 steep shear zones, D_4 ductile thrust	D_2	D_3[a], WFO	$D_{n,\ n-1}$

[a] Re-interpreted in this paper as open domain ii folds.

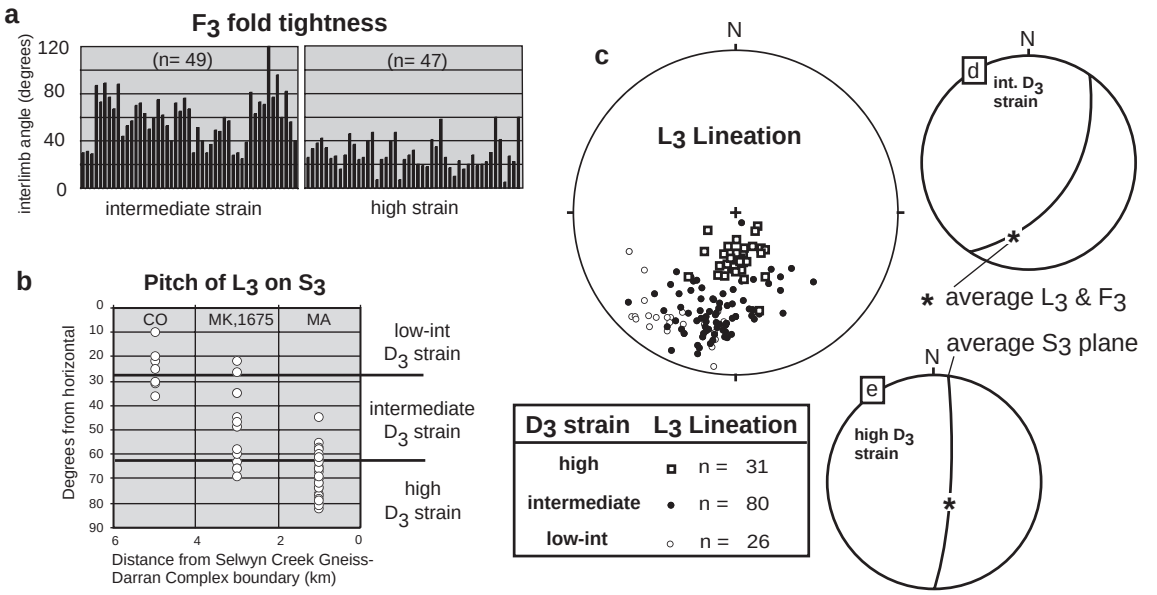

Fig. 9. Structural data from domain iii. (a) Histogram showing variations in the interlimb angle of F_3 folds in intermediate and high strain zones of domain iii. The range of values shown in each plot reflects the heterogeneity of F_3 folding. (b) Plot showing variations in the pitch of L_3 hornblende mineral lineations on S_3 surfaces from west to east across the boundary between domains ii and iii. CO is low strain. MK, and 1675 are intermediate strain. MA is high strain (see Fig. 2 for locations). (c) Lower hemisphere, equal area stereoplot of hornblende mineral lineations (L_3) in domain iii. Note that the L_3 mineral lineations change orientation from shallowly plunging to down-dip with increasing strain. (d and e) Lower hemisphere, equal area stereoplots showing changes in the average orientation of S_3 foliation from west (intermediate strain) to east (high strain) across the boundary between domains ii and iii. Note the S_3 foliation planes rotate counter-clockwise and steepen to near vertical with increasing strain. A steepening of the average orientation of L_3 accompanies this change.

strike to the north parallel to the overall trend of the Darran Complex (Fig. 2).

5. Microstructure

Dioritic gneiss with a high modal proportion of plagioclase facilitated a comparison of plagioclase microstructures in domains i, ii, iii and iv. This comparison allowed us to distinguish the different conditions under which the S_2–L_2 and L_3–S_3 fabrics formed and to show that the L_3–S_3 fabric records mostly subsolidus deformation, consistent with cross cutting relationships indicating that the deformation outlasted magma emplacement.

In domains i and ii coarse subgrains of plagioclase within the S_2 foliation display good crystallographic alignment and sharp grain boundaries that form triple junctions. Plagioclase displays mechanical twins (Fig. 10a) and interlobate–seriate grain boundaries. These textures were produced by the migration of grain boundaries after subgrain formation. Migrating plagioclase grain boundaries were pinned by coarse biotite, indicating that the grain boundary migration postdated some or all of the biotite growth. Plagioclase core–mantle structures are rare in the S_2–L_2 fabric. These textures suggest that dynamic recrystallization of S_2–L_2 plagioclase occurred by dislocation glide and recovery by dislocation climb.

In low strain zones of domain ii plagioclase grains that form part of the S_3–L_3 fabric display deformation twins (albite and lesser pericline), zones of plagioclase subgrains and kink bands (Fig. 10b). In all low strain zones, mechanical twinning in plagioclase formed at the margins of crystals and terminate inwards. Bands of plagioclase subgrains display near parallel extinction, indicating that they once were part of a larger core grain. Kink bands and bent lattice planes in plagioclase indicate that intracrystalline deformation in these low strain areas occurred mainly by dislocation glide and that recovery by dislocation climb was difficult.

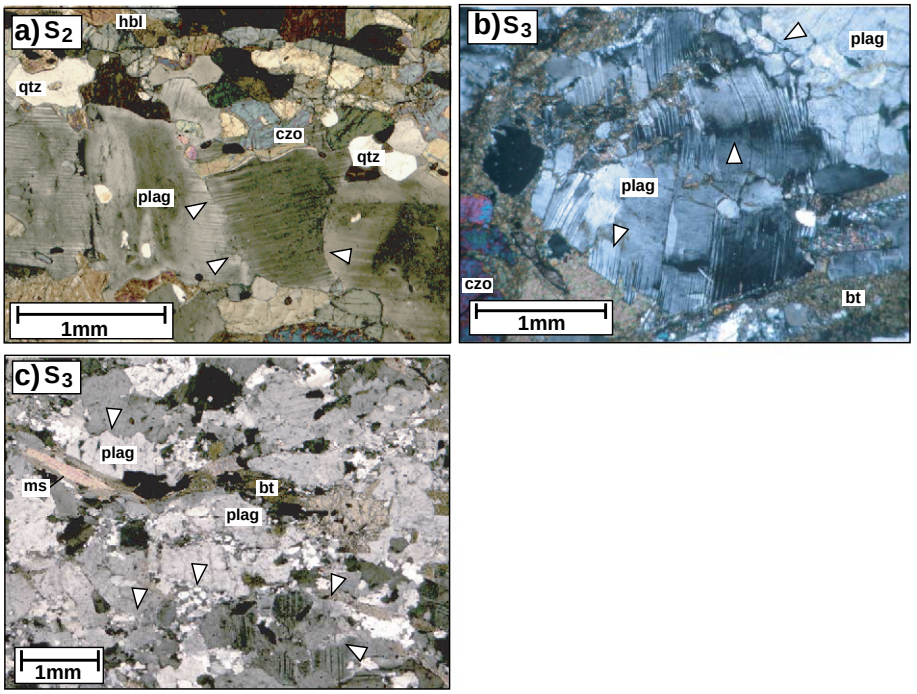

Fig. 10. Photographs of microstructures that form part of the S_2–L_2 and S_3–L_3 fabrics. Images in a and c are from thin sections of surfaces oriented perpendicular to foliation and parallel to lineation. Foliation planes parallel the bottoms of the images unless otherwise indicated. (a) S_2–L_2 in the Mt. Edgar Diorite (LD, domain i, Fig. 2) showing an elongate band of plagioclase containing subgrains with the 001 crystallographic face oriented subparallel to the S_2 foliation. Arrows point to subgrain boundaries that were originally straight and now show evidence of grain boundary migration and mechanical twinning. (b) Mechanical twins and deformation bands in plagioclase from a F_3 fold that displays S_3 axial planar crenulations (from outcrop picture in Fig. 6a, domain ii). Arrow at top right shows plagioclase subgrains that formed along the boundary between two larger grains. Arrow in center shows deformation band that merges into zone of subgrains. Arrow in lower left shows mechanical twins. The image is from a surface oriented perpendicular to the F_3 fold axis. S_3 is parallel to the vertical dimension of the photograph. (c) Core–mantle structures (arrows) in diorite from the Selwyn Creek Gneiss in the Bowen Valley (domain iii, BV, Fig. 2). Note seriate grain boundaries displaying evidence of grain boundary migration (arrow, top left). Mineral abbreviations are as follows: czo=clinozoisite; plag=plagioclase; bt=biotite; hbl=hornblende; ms=muscovite.

In the high strain zones (S_3–L_3) of domains ii and iii, plagioclase crystals display abundant core–mantle structures (Fig. 10c) where core plagioclase grains are surrounded by discontinuous mantles of subgrains that lack internal strain. The strain free crystals suggest that rotational recrystallization and recovery by dislocation climb formed the subgrains. Many of the boundaries between adjacent plagioclase grains and quartz grains also are interlobate and seriate (Fig. 10c), indicating high grain boundary mobility.

These textures reflect the recrystallization of S_2 assemblages within domain iii. The textures suggest that deformation in the Indecision Creek shear zone occurred primarily by recrystallization-accommodated dislocation creep in plagioclase (Tullis and Yund, 1985; Ji and Mainprice, 1990). Granular flow of hornblende also occurred. The dynamic recrystallization of plagioclase indicates that deformation in the shear zone occurred at temperatures of $T > 550$ °C (Olsen and Kohlstedt, 1985; Pryer, 1993). In naturally deformed plagioclase, Kruse and Stunitz (1999) and Rosenberg and Stunitz (2003) showed that plagioclase microstructures similar to those we observed form during dynamic recrystallization at $T = 650$–700 °C. These latter temperature estimates are similar to those obtained using thermobarometric techniques on S_3 mineral assemblages (Clarke et al., 2000; Daczko et al., 2002a,b). Daczko et al. (2002a) obtained metamorphic pressures on S_3 mineral assemblages of $P = 11$–13 kbar. The contrast in plagioclase deformation textures we observed in domain i compared to domains ii and iii suggests that cooling of the lower

crust occurred prior to or during deformation in the shear zone. These results are consistent with the cooling trajectory for the lower crust interpreted by Daczko et al. (2002a).

6. Kinematics

The relationships described in Sections 3 and 4 illustrate the structural changes that accompany an increase in D_3 strain from west to east across domain ii into domain iii. Accompanying this increase in finite strain are systematic changes in the orientation of S_3 and L_3 structures. The S_3 foliation steepens from moderately dipping to the southeast (Fig. 9d) to nearly vertical (Fig. 9e) from west to east. This change in dip is accompanied by a counter-clockwise rotation in the strike of the foliation. In addition, the pitch of L_3 mineral lineations on S_3 surfaces changes from 10–35° in domain ii and relatively low strain areas of domain ii to steeply (55–82°) plunging in high strain areas of domain iii (Fig. 9b and c).

Sense of shear indicators in domains ii and iii allowed us to determine how displacements were partitioned within the shear zone. The best indicators occur at the scale of individual outcrops in domain iii and include asymmetric pods of gneiss, asymmetric boudinage of dikes, oblique foliations and S–C fabric, structures associated with minor shear zones and asymmetric tails on porphyroblasts. Sense of shear indicators were observed on surfaces oriented both oblique and perpendicular to the penetrative hornblende stretching lineations (L_3) observed in domains ii and iii. Where possible, interpretations of shear sense were cross checked using several different types of indicators. Stretched dikes and boudinage indicate that these mineral lineations represent true D_3 stretching directions.

The majority of the high strain zones in domains ii and iii exhibited a subhorizontal sinistral sense of displacement parallel to the northerly strike of steep S_3 foliation planes (e.g. Figs. 6f and 7b). Wandres et al. (1998) described minor shear zones with similar orientations and shear senses in domain iv at Slip Creek (SLIP, Fig. 2). This sense of shear is consistent with the regional-scale counter-clockwise rotation of S_3 foliation planes with increasing strain (compare Fig. 9d and e). However, the orientation of L_3 stretching lineations relative to surfaces displaying maximum asymmetry are different in areas of relatively low (or intermediate) strain compared to areas of high strain. In virtually all high strain zones, structures displayed maximum asymmetry on surfaces oriented perpendicular to foliation and at high angles (60–80°) to down-dip mineral lineations (Fig. 7c). In contrast, in areas of relatively low strain, including in two 1–5 km wide zones at the shear zone margins, structures displayed maximum asymmetry on surfaces oriented perpendicular to foliation and either parallel to or oblique to gently- and moderately-plunging L_3 stretching lineations.

These patterns are consistent with mathematical models that describe finite strain patterns in transpressional shear zones (Jones et al., 2004). The migration of the L_3 stretching lineations toward the down-dip direction of S_3 foliation planes with increasing strain also indicates that, independently of any volume change, pure shear deformation controlled the fabric formation (Lin et al., 1998; Jiang et al., 2001). The contrasting lineation patterns in domains ii and iii suggest that oblique and strike-slip displacements preferentially were partitioned in 1–5 km wide zones at the margins of the shear zone whereas vertical stretching dominated the central part of the shear zone where strains are highest. These patterns also illustrate that the Indecision Creek Shear Zone is characterized by a sinistral component of displacement parallel to the arc combined with components of arc-normal shortening and near vertical extrusion.

7. U–Pb geochronology

To determine the absolute age of deformation and magmatism we analyzed zircon from six dikes from domains ii, iii and iv. Sample locations are shown in Fig. 2, analytical methods are described in the Appendix. Age uncertainties are reported at 2σ and include random and systematic errors.

Sample 0213K4 (Fig. 2) was collected from a dike in domain ii that cuts S_2 foliation and is gently folded by an F_3 fold. These cross cutting relationships indicate that the dike was emplaced after the S_2 foliation had formed and prior to or during F_3 folding. Thirty seven analyses were conducted on zircon cores and tips, yielding two age clusters separated by scattered intermediate ages (Fig. 11a–c). The older cluster,

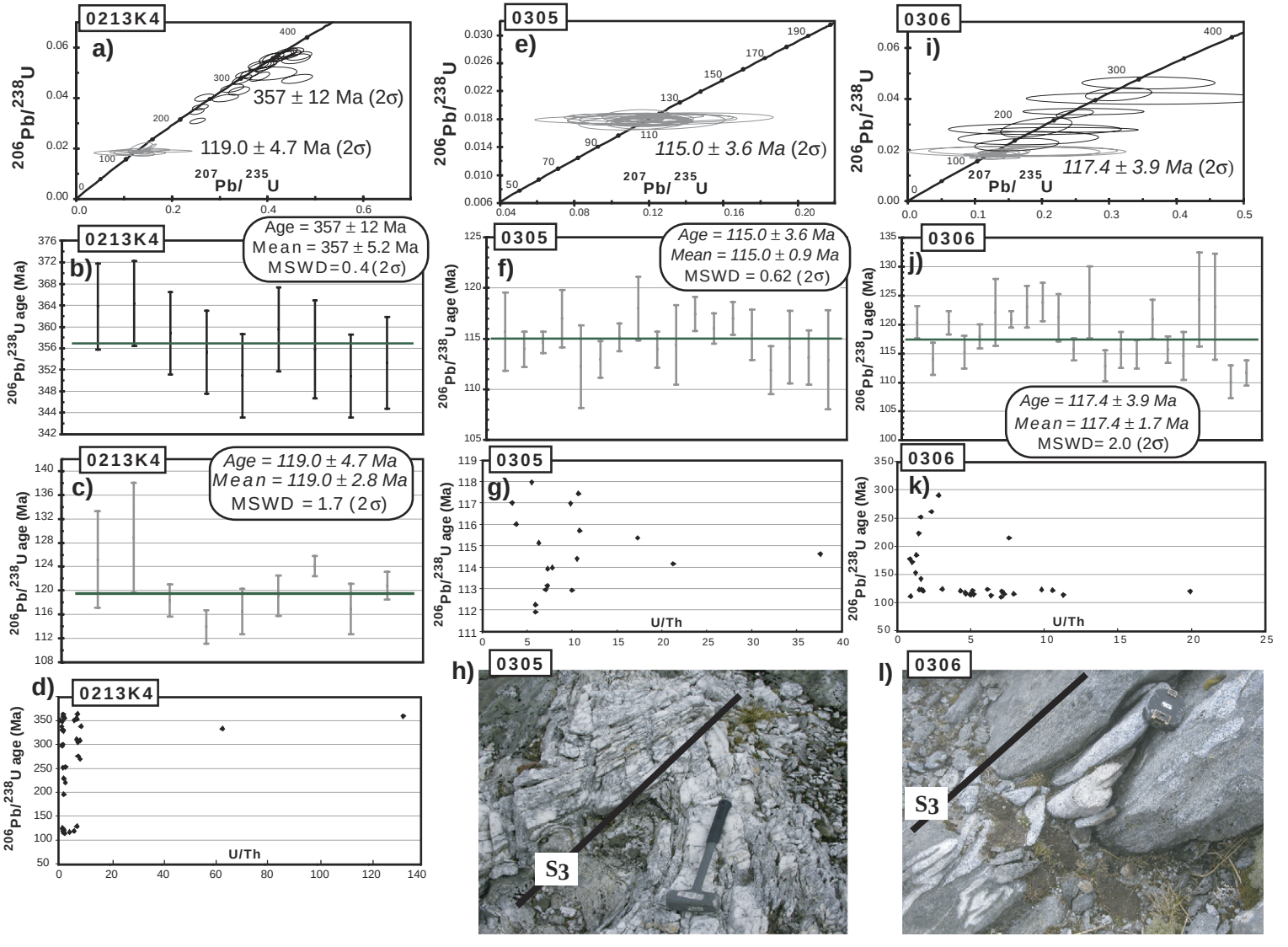
0213K4
a)
357 ± 12 Ma (2σ)
119.0 ± 4.7 Ma (2σ)
206Pb/238U
207Pb/235U
b)
Age = 357 ± 12 Ma
Mean = 357 ± 5.2 Ma
MSWD=0.4(2σ)
206Pb/238U age (Ma)
c)
Age = 119.0 ± 4.7 Ma
Mean = 119.0 ± 2.8 Ma
MSWD = 1.7 (2σ)
d)
U/Th
0305
e)
115.0 ± 3.6 Ma (2σ)
f)
Age = 115.0 ± 3.6 Ma
Mean = 115.0 ± 0.9 Ma
MSWD = 0.62 (2σ)
g)
h)
S3
0306
i)
117.4 ± 3.9 Ma (2σ)
j)
Age = 117.4 ± 3.9 Ma
Mean = 117.4 ± 1.7 Ma
MSWD= 2.0 (2σ)
k)
l)
S3

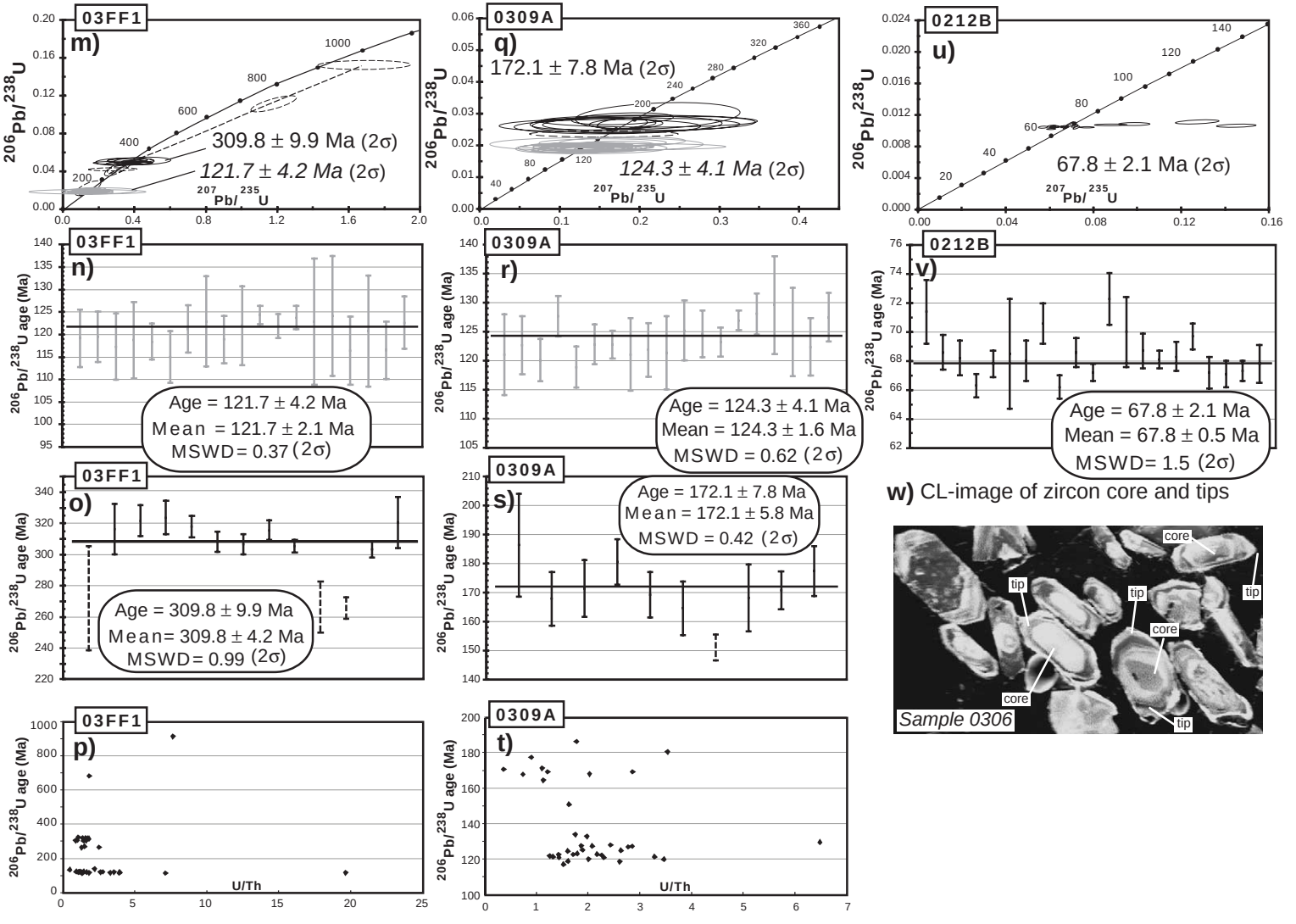
03FF1
m)
309.8 ± 9.9 Ma (2σ)
121.7 ± 4.2 Ma (2σ)
207Pb/235U
206Pb/238U
03FF1
n)
Age = 121.7 ± 4.2 Ma
Mean = 121.7 ± 2.1 Ma
MSWD = 0.37 (2σ)
206Pb/238U age (Ma)
03FF1
o)
Age = 309.8 ± 9.9 Ma
Mean = 309.8 ± 4.2 Ma
MSWD = 0.99 (2σ)
03FF1
p)
U/Th
0309A
q)
172.1 ± 7.8 Ma (2σ)
124.3 ± 4.1 Ma (2σ)
0309A
r)
Age = 124.3 ± 4.1 Ma
Mean = 124.3 ± 1.6 Ma
MSWD = 0.62 (2σ)
0309A
s)
Age = 172.1 ± 7.8 Ma
Mean = 172.1 ± 5.8 Ma
MSWD = 0.42 (2σ)
0309A
t)
U/Th
0212B
u)
67.8 ± 2.1 Ma (2σ)
0212B
v)
Age = 67.8 ± 2.1 Ma
Mean = 67.8 ± 0.5 Ma
MSWD = 1.5 (2σ)
w) CL-image of zircon core and tips
core
tip
Sample 0306

generally from the cores of grains, yielded an age of 357 ± 12 Ma. Tips yielded younger ages, with a mean of 119.0 ± 4.7 Ma. The older age is interpreted to be the age of crystallization of inherited zircon cores. The younger age is interpreted as the age of the growth of the zircon rims. The low (1–7) U/Th ratios of the analyses, except for two ~350 Ma core analyses (Fig. 11d), suggest that the rims have an igneous origin, although this distinction is not critical for estimating the ages of the rock fabrics (see discussions provided by Rubatto et al., 2001; Williams, 2001). The older cluster of ages from inherited cores suggests that the dike was emplaced into Paleozoic (~350 Ma) crust of the Gondwana continental margin (inboard or western terrane). The ages and field relationships from this sample suggest that D_3 deformation in domain ii outlasted the emplacement of the 119.0 ± 4.7 Ma dike.

In domain iii, samples 0305 and 0306 were collected from dikes that are folded by F_3 folds. Sample 0305 is from a tightly folded biotite-bearing pegmatitic dike (Fig. 11h) that cuts igneous layering in a gabbroic pod within the Harrison Gneiss. Sample 0306 is from an isoclinally folded, biotite-bearing dioritic dike (Fig. 11l) that is transposed parallel to S_3 in the Indecision Creek Shear Zone. Both of these dikes display a foliation (S_3) that parallels the axial planes of the F_3 folds. These relationships indicate that the dike yielding sample 0305 was emplaced during D_3 shear zone deformation and that the dike yielding sample 0306 was emplaced prior to D_3.

Sample 0305 contained a single population of zircon cores that yielded a mean age of 115 ± 3.6 Ma (Fig. 11e,f). All zircon grains displayed high U/Th ratios (5–20) and high U concentrations (average of ~970 ppm) with an outlier showing a U/Th ratio of 37 (Fig. 11g). These high values are consistent with a metamorphic origin for the zircon, although this is difficult to confirm because all the values are high and the sample yielded only one population. The results suggest that D_3 deformation began before and outlasted the 115 ± 3.6 Ma age of this sample. Sample 0306 contained core zircon that yielded a 300–150 Ma age range and a cluster of younger tips and rims that yielded a mean age of 117.4 ± 3.9 Ma (Fig. 11i,j). This sample displayed low U/Th ratios in cores that were overgrown by rims (Fig. 11w) displaying 1–20 U/Th ratios (Fig. 11k). The range of old core ages suggests that they are a combination of >300 Ma zircon and the younger, Cretaceous overgrowths of either igneous or metamorphic origin.

Sample 03FF1 is from a dioritic dike that intruded the George Sound Shear Zone (Fig. 1), and represents the first attempt to date this feature. This shear zone is a steep north-striking upper amphibolite facies shear zone that cuts igneous layering within the Western Fiordland Orthogneiss at Anchorage Cove in George Sound. The igneous layering is interpreted to be equivalent to the S_2 foliation in northern Fiordland (domain i). The dike displayed a weak to moderate foliation (S_3) that parallels the margins of the shear zone. These relationships indicate that this dike was emplaced during or after the formation of S_2 and during the formation of the S_3. This sample yielded two zircon populations with a mean core age of 309.8 ± 4.2 Ma and a mean rim and tip age of 121.7 ± 4.2 Ma (Fig. 11m, n and o). Core and rim analyses show mostly low U/Th (<4), except for two rim analyses (Fig. 11p). There are also two core analyses that yielded Late Precambrian ages. The young rims tend to show U/Th ratios that are higher than in the older analyses, suggesting that some of the rims are metamorphic. The distinct clustering of the two age groups suggests that ~121 Ma metamorphic or igneous zircon grew over inherited Paleozoic and late Precambrian cores.

Fig. 11. U–Pb isotopic data from zircon collected using laser-ablation ICPMS. Plots a, e, i, m, q, and u are concordia plots that show all analyses from samples 0213K4, 0305, 0306, 03FF1, 0309A, 0212B. See Fig. 2 for sample locations. Error ellipses on these plots are at the 1σ level, ages are shown at the 2σ level. An explanation of methods is provided in the appendix. Plots b, c, f, j, n, o, r, s, and v show $^{206}Pb/^{238}U$ ages, which are the important ages for samples this young. Two plots are shown for the samples that yielded two age groups. The ages are shown with two uncertainties; those labeled "age" include all errors, whereas the "mean" includes only the random (measurement) errors. The larger uncertainty is reported as the age of the grains in the text. Note that these uncertainties are shown at 2σ levels, whereas the error bars for individual analyses are shown at 1σ levels. Plots (d, g, k, p, t) of U/Th versus $^{206}Pb/^{238}U$ ages also are shown. These plots help discriminate between igneous and metamorphic zircon. See text for explanation. Photographs (11h and 11l) illustrate the field relationships of samples 0306 and 0305, respectively. Both samples are from folded (F_3) dikes where fold axes plunge steeply to the southeast. See text for interpretation. Fig. 11w shows a cathode luminescence image of zircon grains displaying zoned cores and overgrowths (tips) analyzed from sample 0306.

Sample 0309A was collected from a medium grained biotite-bearing diorite from Mt. Mitchelson near the boundary between domain iii and iv (MM, Fig. 2). The sample is from the xenolith-free interior of a 50 m wide dike in the Selwyn Creek Gneiss. The sample was collected from the outcrop pictured in Fig. 8b. The dike cuts host gabbro that is interpreted part of the Darran Complex. The age of this dike emplacement provides a minimum age of magmatism within the Selwyn Creek Gneiss.

Nine zircon grains were analyzed from sample 0309A. These grains included oscillatory-zoned cores that are truncated by younger tip and rim growths. Core grains yielded a mean age of 172.1 ± 7.8 Ma and younger tips and rims yield a mean age of 124.3 ± 4.1 Ma (Fig. 11q, r and s). Both populations of zircon show low values of U/Th (0.5–3.5, Fig. 11t), suggesting that both are of igneous origin. We interpreted the 172.1 ± 7.8 Ma cores as reflecting zircon inherited from a host or source rock and the 124.3 ± 4.1 Ma rims as the age of igneous zircon growth and crystallization.

Sample 0212B is from a dioritic dike that was emplaced into a D_3 shear zone along the deformed margin between the Pembroke Granulite and Milford Gneiss exposed in Stirling Valley (Fig. 2). The margins of the dike cut S_3 foliation in the adjacent orthogneiss. The dike is openly folded with white mica aligned in the hinges of the folds. Twenty-one analyses were conducted on core regions of zircon grains from this sample. These analyses produced similar $^{206}Pb/^{238}U$ ages but highly variable $^{206}Pb/^{207}Pb$ ages due to the low concentrations of ^{207}Pb in the young zircon grains. The $^{206}Pb/^{238}U$ ages yielded a mean age of 67.8 ± 2.1 Ma (Fig. 11u,v). These results suggest that the dike was emplaced after deformation in the Indecision Creek Shear Zone terminated.

8. Discussion

In this section we develop a model of partitioned transpression for northern Fiordland. We also interpret the age of magmatism, metamorphism and deformation and discuss the relationship between transpression and magmatism in the lower crust.

8.1. Model of partitioned transpression

The 12–15 km wide Early Cretaceous Indecision Creek Shear Zone forms a major tectonic boundary between high-pressure gneisses of the Fiordland granulite belt and the middle to upper crustal rocks of the Darran Complex. Variations in finite strain suggest that the boundaries of the shear zone are vertical and parallel the overall trend of the arc. Tight and isoclinal folds record a minimum of 60% shortening normal to the arc in zones of high strain. Shear zone structures also record components of arc-parallel sinistral strike-slip and oblique-slip displacements and near vertical extrusion.

Some of the structural patterns we observed are similar to those predicted by mathematical models of transpression. With increasing strain the pitch of lineations on foliation surfaces changes from oblique (10–35°) to down-dip (55–82°) and foliation planes steepen and rotate counter-clockwise (Figs. 9 and 12b). These patterns are consistent with models that indicate that pure shear deformation accumulates more rapidly than simple shear deformation so that pure shear is expected to dominate at high strains (Lin et al., 1998; Jiang et al., 2001). However, unlike in most mathematical models, our results show that the deformation was extremely heterogeneous (Fig. 12a). The variations do not occur smoothly across the margin of the shear zone, but instead reflect a complex partitioning of displacements. Foliations define a network of discontinuous and branching high strain zones, disharmonic folds are common, and the planes on which structures display maximum asymmetry varies greatly. Nevertheless, the patterns are clear enough to indicate an environment of partitioned transpression for northern Fiordland. Our results indicate that stretching lineations can track, albeit imperfectly, a progressive increase in finite strain in natural shear zones that form within arcs.

Some of the patterns we observed also are in agreement with models of inclined transpression as defined by Jones et al. (2004). In these models, the pitch of lineations on foliation planes is variable and there is abundant evidence of simultaneous arc-normal contraction and oblique-slip displacements. In the case of Fiordland, the oblique-slip deformation is partitioned further such that most of the dip-slip displacement occurs in high strain zones in domain iii.

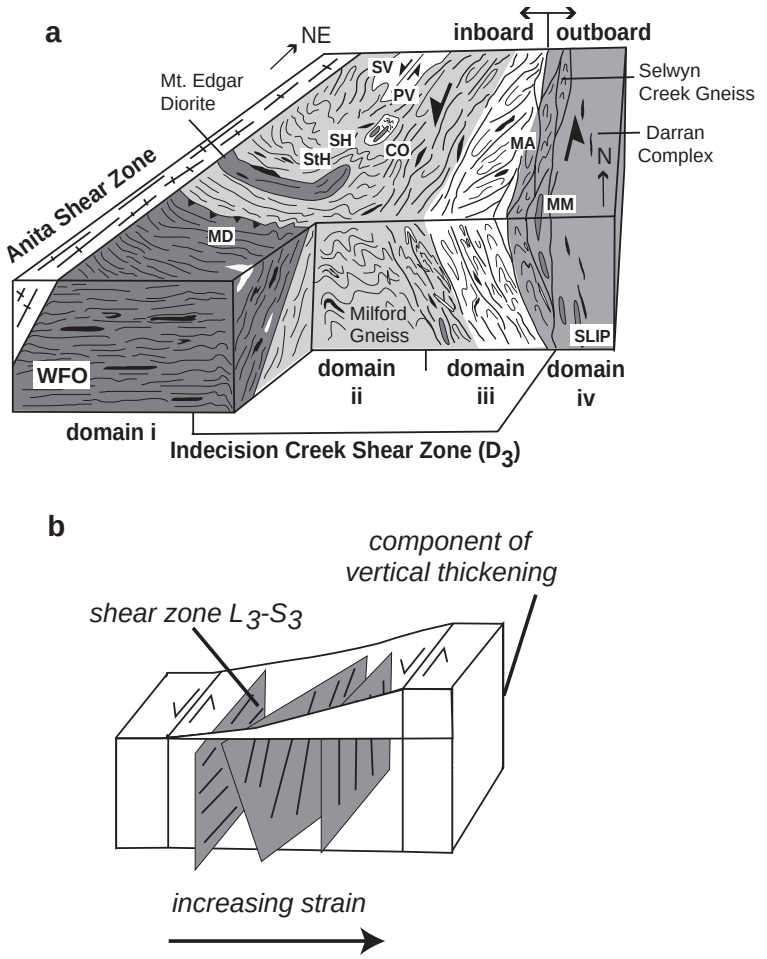

Fig. 12. Block diagram showing the geometry of structures in the Indecision Creek Shear Zone. (a) Cut away diagram illustrating a model of partitioned transpression in northern Fiordland. WFO is Western Fiordland Orthogneiss, other abbreviations are same as in Fig. 2. (b) Schematic diagram showing variations in the orientation of L_3 stretching lineations in the Indecision Creek Shear Zone.

However, unlike inclined transpression, the Indecision Creek Shear Zone is vertical and no normal-displacements were observed in the shear zone. We therefore prefer a model of transpression where sinistral oblique-slip and dip-slip displacements are partitioned within the margins of the shear zone and fabrics controlled by the coaxial component of the deformation dominate the high strain central parts of the shear zone. This model is similar to that proposed by Tavarnelli et al. (2004) for the southern Uplands of Scotland where transpression involved partitioning into a central contraction-dominated zone that is bounded on both sides by strike-slip-dominated zones. Folding also plays an important role in accommodating the shortening in the model for Scotland. These similarities suggest that zones of partitioned transpression where crustal anisotropies control deformation patterns are important not only in the upper crust but also in the lower crust of arcs.

The three-dimensional variability of deformation in the Indecision Creek Shear Zone indicates that there was no instantaneous switch in lineation direction from horizontal to vertical during the deformation. Czeck and Hudleston (2003) suggest that variations in the direction of stretch associated with the pure shear component of deformation can produce multiple lineation orientations across a shear zone. These variations can result from anastamosing networks of

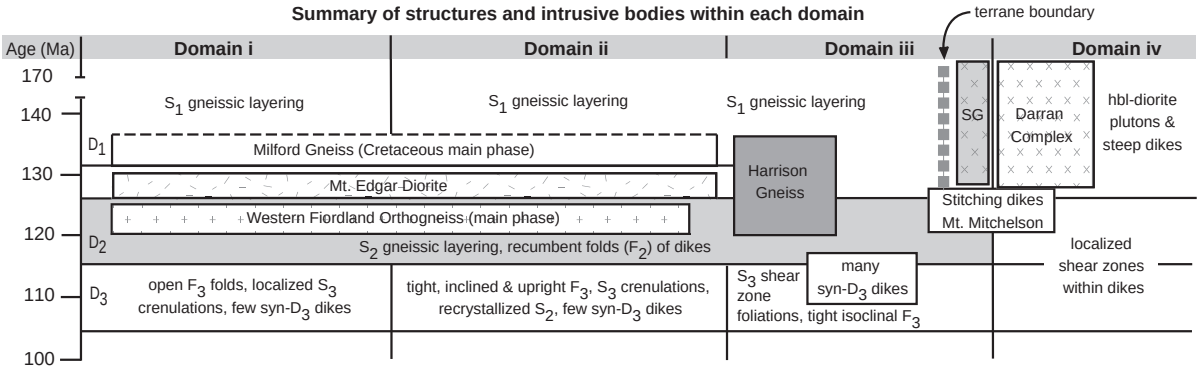

Fig. 13. Time–space diagram illustrating the sequence of deformation and igneous intrusions within each structural domain. Note terrane boundary (vertical dashed line) that separates outboard (right) and inboard (left) belts of igneous rock. Diagram shows two magmatic trends: a continentward migration of magmatic activity after ~140 Ma and focused magma emplacement in the Indecision Creek Shear Zone (D_3, domain iii) after ~119 Ma.

shear zone fabrics or from local pressure gradients around zones of rigid material (such as ultramafic pods). The heterogeneous lozenge-shaped structure of the Indecision Creek Shear Zone where strain intensities are variable supports this interpretation for northern Fiordland. Vertical lineations may result where pure shear deformation controls fabric formation at high strains and oblique lineations result where simple shear dominates at low strains (Czeck and Hudleston, 2004). The relatively low strains that characterize domain ii compared to domain iii and the occurrence of oblique lineations in the former domain support this interpretation of the origin of the lineation orientations in northern Fiordland. Nevertheless, temporal variations in the style, intensity and position of deformation may also have contributed to the structural variability in the shear zone. Detailed kinematic vorticity studies to determine the exact contributions of pure versus simple shear in different places may allow these interpretations to be tested in the future.

Finally, the occurrence of a steep, transpressional shear zone along the boundary between lower crustal rocks to the west and middle and upper crustal rocks to the east raises the possibility that vertical extrusion in the shear zone caused this structural break. This differs from the conventional view that exhumation was controlled by extensional structures (Oliver, 1990; Gibson and Ireland, 1995). However, it is unlikely that vertical extrusion can explain the exhumation of whole terrane because of its narrow spatial extent. Instead, we suggest that the change in paleodepth across this boundary resulted from a combination of underthrusting of Darran Complex beneath the Gondwana margin (see also Muir et al., 1998) and a minor component of vertical displacement. This underthrusting was accompanied by the migration of the locus of magmatism continentward as the outboard terrane converged with the continental margin (Figs. 13 and 14). With increasing strain, it is probable that the shear zone steepened into its present vertical orientation. This model is in agreement with the definition of an originally inclined zone of deformation that accompanied underthrusting and later evolved into a vertical transpressional shear zone. These inter-

Fig. 14. Tectonic model for the evolution of the Median Batholith during the Mesozoic (modified from Tulloch and Kimbrough, 2003; Klepeis et al., 2004). (a) Outboard (eastern) belt of the Median Batholith is emplaced (mostly 168–137 Ma). Accretion of Eastern Province terranes occurs in the Late Jurassic (after Mortimer et al., 1999b). (b) Inboard (western) belt is emplaced mainly within the Gondwana margin (129–105 Ma), with satellite intrusions emplaced into the outboard belt. (c) Crustal shortening, burial and thickening follows the emplacement of the inboard belt. Oblique convergence results in the formation of the transpressional Indecision Creek and George Sound shear zones. The Indecision Creek Shear Zone separates the outboard belt from continental margin rocks that were intruded by the inboard belt. Small volumes of magma are emplaced into and move through the vertical shear zones as magmatism and compression diminish. DC is the Darran Complex; SG represents plutons of the Selwyn Creek Gneiss; HG is Harrison Gneiss, MG is Milford Gneiss, WFO is Western Fiordland Orthogneiss; MED is Mt. Edgar Diorite; CO is Camp Oven Creek; DA is Devil's Armchair; MM is Mt. Mitchelson. Asterisk (*) denotes new ages presented in this paper.

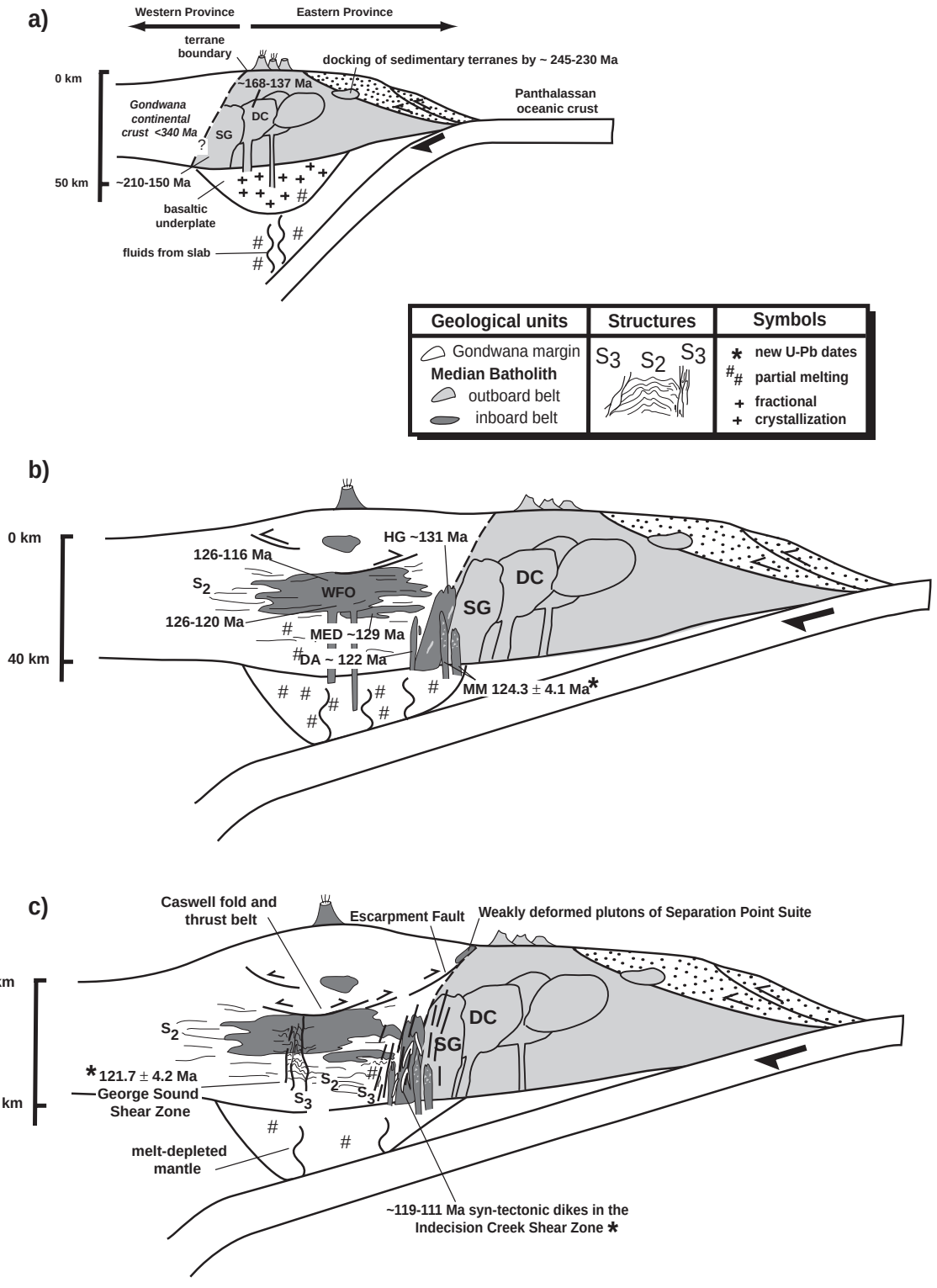
a)
Western Province
Eastern Province
terrane boundary
docking of sedimentary terranes by ~ 245-230 Ma
0 km
~168-137 Ma
Panthalassan oceanic crust
Gondwana continental crust <340 Ma
DC
SG
?
50 km
~210-150 Ma
basaltic underplate
fluids from slab
Geological units
Gondwana margin
Median Batholith
outboard belt
inboard belt
Structures
S3 S2 S3
Symbols
new U-Pb dates
partial melting
fractional crystallization
b)
0 km
126-116 Ma
HG ~131 Ma
S2
WFO
DC
SG
126-120 Ma
MED ~129 Ma
40 km
DA ~ 122 Ma
MM 124.3 ± 4.1 Ma*
c)
Caswell fold and thrust belt
Escarpment Fault
Weakly deformed plutons of Separation Point Suite
0 km
S2
DC
SG
*121.7 ± 4.2 Ma
George Sound Shear Zone
S2
S3
S3
40 km
melt-depleted mantle
~119-111 Ma syn-tectonic dikes in the Indecision Creek Shear Zone *

pretations suggest that the Indecision Creek Shear Zone is the lower crustal equivalent of the intra-arc Escarpment fault located on Stewart Island (Figs. 2 and 14c).

8.2. The age of magmatism, metamorphism and deformation

The results of zircon analyses from domains ii, iii and iv allowed us to estimate the location of a boundary between the inboard (western) and outboard (eastern) terranes (Figs. 13 and 14). The oldest cluster of ages from sample 0213K4 in domain ii indicates that this dike sampled Carboniferous material. This result is consistent with interpretations that the Milford Gneiss contains a mixture of Paleozoic rock of the Gondwana continental margin and Mesozoic igneous rock (see also Tulloch et al., 2000). Hollis et al. (2003) obtained a similar 346 ± 6 Ma protolith age from Camp Oven Creek, which lies on the western side of domain iii. Klepeis et al. (2004) also obtained a 365.3 ± 11.4 Ma crystallization age from near Mt. Kepka (MK, Fig. 2) on the western side of domain iii due south of Camp Oven Creek. In contrast, samples located in domain iv (sample 0309A, Fig. 2) and on the eastern side of domain iii (MA, Fig. 2) yielded Late Jurassic or younger crystallization ages and no sign of Paleozoic inheritance. These ages are similar to the dominant range of ages from the Darran Complex (Muir et al., 1998). The contrast in ages indicates that dikes on either side of domain iii sampled distinctive crustal materials (Fig. 14a). The pattern suggests that the boundary between the inboard (western) and outboard (eastern) terranes lies within domain iii and that the Indecision Creek Shear Zone reactivated this crustal boundary during the Early Cretaceous (Figs. 12 and 14c).

The results of U–Pb geochronology also reveal two magmatic trends within the deep crust of the Median Batholith. First, the continentward progression of magmatism after ~140 Ma (Fig. 14a,b) corresponds to the shift from magma emplacement in the outboard belt to that the inboard belt described by Tulloch and Kimbrough (2003). Second, and new to this study, is that the data record focused magmatism, in the form of syntectonic dikes, in the Indecision Creek Shear Zone after ~119 Ma (Fig. 13).

Sample 0309A from the near vertical dioritic dike at the eastern end of domain iii (Figs. 2 and 8) yielded the youngest crystallization ages (124.3 ± 4.1 Ma) yet obtained from the deformed western margin of the Darran Complex. These dikes were emplaced at the same time as the Western Fiordland Orthogneiss (using the U–Pb ages reported by Hollis et al., 2004) and the vertical Devil's Armchair dike (Hollis et al., 2003) at Camp Oven Creek (Fig. 2). These young intrusions form part of the inboard belt of Tulloch and Kimbrough (2003). The fact that they intrude both Paleozoic rock of the inboard terrane at Camp Oven Creek and Jurassic rock of the outboard terrane at Mt. Mitchelson (stitching dikes, Fig. 13) indicates that these two terranes were in close proximity prior to formation of the Indecision Creek Shear Zone (by at least ~129 Ma according to Hollis et al., 2003).

The igneous rim ages obtained from domain ii (119.0 ± 4.7 Ma, sample 0213K4) are similar to metamorphic ages found throughout the Arthur River Complex (Tulloch et al., 2000; Hollis et al., 2003). The metamorphic ages are interpreted to reflect zircon growth or recrystallization due to the thermal effects accompanying the emplacement of the Western Fiordland Orthogneiss at ~120 Ma. We suggest that the similar ages we obtained reflect magmatic activity that occurred synchronously with this event. These ages place a lower limit on the age of D_3 deformation in the Indecision Creek Shear Zone. The young ages obtained from zircon tips from domain ii (samples 0305 and 0306) and field relationships (Fig. 11h and l) indicate that the deformation outlasted emplacement of the 115.0 ± 3.6 Ma dike. Klepeis et al. (2004) suggested that deformation in the Indecision Creek Shear Zone lasted from 116–105 Ma on the basis of regional relationships. The ~105 Ma age, reported by Tulloch and Kimbrough (2003), is the age of the youngest arc-related plutons of the inboard belt. Our data are consistent with this age range, although they allow the deformation to have begun as early as ~119 Ma and to have ended in the lower crust by ~111 Ma (Fig. 13). This latter age is consistent with the results of Flowers et al. (2005) who concluded that isobaric cooling from $T > 750$ °C through 550–650 °C occurred through the interval 111–113.5 Ma.

Sample 03FF1 is the first sample from the George Sound Shear Zone (Fig. 1) that has been dated using

U–Pb techniques. Klepeis et al. (2004) correlated deformation in the George Sound Shear Zone with that in the Indecision Creek Shear Zone on the basis of similarities in structural style. The crystallization or metamorphic age (121.7 ± 4.1) we obtained support this correlation, although they allow the George Sound Shear Zone to have formed slightly earlier than the Indecision Creek Shear Zone. The old (309.8 ± 9.9 Ma) inherited cores obtained from this sample are similar to those obtained from the George Sound paragneiss by Hollis et al. (2004). The young ages are similar to Cretaceous metamorphic rims on detrital zircon cores from this same unit obtained by Hollis et al. (2004).

The 67.8 ± 2.1 Ma age obtained from sample 0212B in a weakly deformed sample is much younger than most U–Pb ages reported from northern Fiordland. Hollis et al. (2003) reported an 81.8 ± 1.8 Ma age from a post-tectonic dike near where we collected our sample. They correlated this age with extensional magmatism that accompanied the opening of the Tasman Sea during the Late Cretaceous. It is possible that ~68 Ma growth of zircon reflected fluid flow through the rifted continental margin of western New Zealand.

8.3. Relationship between transpression and magmatism

Geochronologic data indicate that some of the youngest dikes in Fiordland were emplaced into the center of the Indecision Creek Shear Zone during transpression. This result, combined with abundant evidence of syntectonic dike emplacement (e.g. Figs. 6f,7a,11h), invites a comparison of our field data with models that predict transpression is an efficient mechanism for transporting magma through the lithosphere. The microstructural evidence of subsolidus deformation indicates that deformation in the shear zone outlasted dike emplacement.

The kinematic patterns preserved within the Indecision Creek Shear Zone (summarized in Fig. 12) indicate that lower crustal material, including magma, was extruded vertically or nearly so during deformation. During transpression material may flow upward because pressure gradients created by buoyancy forces and differential stress are greatest in this direction (Saint Blanquat et al., 1998). However, there are numerous ways, including the effects of rheological contrasts, in which local pressure gradients may also result in non-vertical extrusion of material at some scales (Czeck and Hudleston, 2004). The dominance of oblique lineations in the Indecision Creek Shear Zone suggests that non-vertical transport was an important process.

The exact pathways of magma movement in shear zones at length scales of a few kilometers or more typically are difficult to interpret on the basis of field relationships alone. Klepeis and Clarke (2004) described relationships at Camp Oven Creek whereby foliation planes (identical to the S_3 foliation described here) and vein networks were exploited as pathways for melt migration. This exploitation of foliation planes as pathways was indicated by discordant, undeformed leucosome that paralleled the axial planes of folds in migmatitic dioritic gneiss (see their Fig. 7c). The relationships described in this paper indicate that magma in the form of dikes and veins was considerably more complex. We observed dikes that were emplaced both parallel to, oblique to and orthogonal to S_3 foliation planes (Fig. 7a). This implies that the steep orientation of the S_3 foliation influenced the geometry of some but not all dikes that were emplaced during the deformation. The emplacement of magma into jogs created by curved shear zones, such as those described in other orogens (Klepeis and Crawford, 1999), can be ruled out as a mechanism for magma emplacement in the Indecision Creek Shear Zone.

Despite the uncertainty in specific pathways for magma migration, the occurrence of focused syntectonic magmatism in the Indecision Creek Shear Zone implies that the deformation was aided in the transfer and emplacement of some magma within the lower crust. The age of the youngest dikes that were emplaced into the lower crust during convergence is ~111 Ma. Young (~116 Ma) intrusive bodies occur elsewhere in Fiordland (Tulloch and Kimbrough, 2003; Hollis et al., 2004), but the greatest number of syntectonic dikes discovered so far in northern Fiordland occur in the shear zone (Figs. 13 and 14c). This relationship implies that magma moved into and possibly through the shear zone to shallow crustal levels where arc-related magmatism continued until ~105 Ma (Tulloch and Kimbrough, 2003). However, the small size and low percentage of the syntectonic dikes observed in the shear zone, the lack of large layered complexes or batholiths in the lower,

middle and upper crust at this time, suggest that the overall volume of magma that was emplaced into the shear zone after ~120 Ma probably remained small. This also is implied by the excellent preservation of shear zone fabrics, which tend to be erased by magmatic activity. We therefore suggest that transpression resulted in the movement of only a small volume of magma to shallower crustal levels.

9. Conclusions

The Median Batholith is composed of an eastern belt that originally formed outboard of the Gondwana continental margin during the Early Mesozoic, and an inboard (western) belt that includes dikes and layered igneous complexes that intruded the continental margin. We show that a transpressional style of intra-arc deformation evolved in the lower crust (~45 km paleodepth) as these two provinces accreted onto the Gondwana margin during convergence. Zircon populations from dikes allowed us to identify the approximate location of the boundary between the outboard and inboard terranes. This boundary was reactivated by the near vertical Indecision Creek Shear Zone during the waning stages of arc magmatism. Steep ~120 Ma dikes that predate the shear zone intrude both Paleozoic rock of the inboard terrane and Jurassic rock of the outboard terrane, confirming that these two terranes were in close proximity prior to formation of the shear zone.

The Indecision Creek Shear Zone is 12–15 km wide, nearly vertical and parallels the overall trend of the Median Batholith. Systematic changes in the three-dimensional orientation of foliations and lineations occur within the shear zone. Foliation planes rotate counter-clockwise and steepen from moderately dipping to nearly vertical with increasing strain. The pitch of mineral lineations on foliation surfaces changes from 10–35° in areas of relatively low and intermediate strain zones to 55–82° in high strain zones. Sense of shear indicators indicate that the shear zone records a sinistral component of displacement parallel to the arc combined with components of arc-normal shortening (a minimum of 60% in high strain zones) and vertical extrusion. A migration of shear zone stretching lineations toward vertical with increasing strain suggests that the boundary normal component (pure shear) of the deformation controlled fabric formation at high strains. Strike-slip and oblique-slip deformation preferentially was partitioned at the boundaries of the shear zone. This style of deformation partitioning was controlled by rheological contrasts that resulted from the steep orientations of dikes and the boundary between outboard and inboard terranes, and differences in composition and crustal temperature across this boundary.

U–Pb geochronology indicates that at least two large transpressional shear zones developed in the lower crust after ~119 Ma until at least ~111 Ma. During this period, transpressional deformation aided the transport of magma through the lower crust. U–Pb dates indicate that these vertical shear zones formed in the lower crust at the same time as intra-arc reverse faults formed in the middle and upper crust. In contrast, no major strike-slip faults have been identified at upper crustal levels.

Geochronologic and structural data indicate that transpressional deformation facilitated the movement of small amounts of magma through the lower crust. Some of the youngest magmatism in Fiordland occurred at the center of the Indecision Creek Shear Zone. The pattern of magma transfer during transpression was complex and involved the emplacement of magma both parallel to and across shear zone foliations. The size of the intrusions observed in northern Fiordland suggests that the total volume of magma emplaced during transpression was small. This probably resulted from the occurrence of the deformation during the waning stages of arc magmatism as convergence slowed and finally stopped.

Acknowledgments

This paper represents part of the Master of Science thesis of SBM at the University of Vermont. Funding to support this work was provided by National Science Foundation funding to KAK (EAR-0087323 and EAR-0337111), Australian Research Council funding to GLC (ARC-A10009053), and funding from the Geological Society of America's Pretorius Fund. We thank A. Tulloch, N. Mortimer and I. Turnbull for discussions and assistance. We thank the Department of Land Conservation in Te Anau for permission to visit and sample localities in the Fiordland National Park. Michael Bailey and W.C. Simonson provided assis-

Table 2
U–Pb (zircon) geochronologic analyses by laser-ablation multicollector ICP mass spectrometry

						Isotopic ratios					Apparent ages (Ma)					
Sample–grain	U (ppm)	$^{206}Pb/^{204}Pb$	U/Th	$^{207}Pb^*/^{235}U$	± (%)	$^{206}Pb^*/^{238}U$	± (%)	Error corr.	$^{206}Pb/^{207}Pb$	± (%)	$^{206}Pb^*/^{238}U$	± (Ma)	$^{207}Pb^*/^{235}U$	± (Ma)	$^{206}Pb^*/^{207}Pb^*$	± (Ma)
0306—1T	876	3588	19.9	0.12178	9.20	0.01885	2.28	0.25	21.341	8.91	120.4	2.8	117	11	42	107
0306—1C	*41*	*2377*	*1.3*	*0.19315*	*17.80*	*0.02905*	*8.00*	*0.45*	*20.739*	*15.90*	*184.6*	*15.0*	*179*	*34*	*110*	*188*
0306—1T2	1144	9901	11.3	0.12579	6.72	0.01785	2.42	0.36	19.567	6.27	114.1	2.8	120	9	246	72
0306—2T	849	12136	7.1	0.13093	6.32	0.01885	1.67	0.26	19.846	6.09	120.4	2.0	125	8	213	71
0306—2C	*100*	*857*	*1.0*	*0.23150*	*31.89*	*0.02708*	*2.07*	*0.06*	*16.128*	*31.83*	*172.2*	*3.6*	*211*	*72*	*674*	*340*
0306—2T2	1286	12,970	5.2	0.12485	6.98	0.01804	2.47	0.35	19.922	6.53	115.3	2.9	119	9	204	76
0306—3T	773	15,158	4.6	0.13011	7.88	0.01847	1.75	0.22	19.569	7.69	118.0	2.1	124	10	245	89
0306—3C	*60*	*1022*	*0.9*	*0.19043*	*44.44*	*0.02792*	*4.95*	*0.11*	*20.212*	*44.17*	*177.5*	*8.9*	*177*	*82*	*170*	*516*
0306—3T2	329	2244	10.6	0.14478	17.21	0.01912	4.73	0.27	18.209	16.55	122.1	5.8	137	25	409	185
0306—4C	*366*	*12860*	*7.6*	*0.24795*	*7.00*	*0.03392*	*3.10*	*0.44*	*18.864*	*6.28*	*215.1*	*6.8*	*225*	*17*	*329*	*71*
0306—5T	1055	17,059	4.3	0.13235	4.05	0.01893	1.14	0.28	19.723	3.88	120.9	1.4	126	5	227	45
0306—5T2	948	11,258	9.8	0.13426	6.96	0.01928	2.90	0.42	19.799	6.33	123.1	3.6	128	9	218	73
0306—6T	945	8902	6.1	0.12941	7.88	0.01941	2.69	0.34	20.678	7.41	123.9	3.4	124	10	117	87
0306—6T2	337	8386	5.1	0.14521	16.12	0.01898	3.35	0.21	18.021	15.77	121.2	4.1	138	23	432	176
0306—7T	795	9076	7.3	0.12949	4.93	0.01811	1.64	0.33	19.281	4.65	115.7	1.9	124	6	279	53
0306—7C	54	2111	1.6	0.15112	75.04	0.01939	4.98	0.07	17.695	74.88	123.8	6.2	143	109	473	828
0306—8T	1084	16,643	6.4	0.11893	5.57	0.01767	2.36	0.42	20.480	5.04	112.9	2.7	114	7	140	59
0306—8C	*172*	*2511*	*1.5*	*0.26161*	*22.73*	*0.03526*	*2.02*	*0.09*	*18.582*	*22.64*	*223.4*	*4.6*	*236*	*59*	*363*	*255*
0306—8T2	1383	12,645	4.7	0.11833	6.87	0.01810	2.66	0.39	21.095	6.33	115.7	3.1	114	8	70	75
0306—9t	580	3540	5.0	0.12424	8.87	0.01798	2.12	0.24	19.957	8.61	114.9	2.5	119	11	200	100
0306—9C	*127*	*2971*	*2.8*	*0.36048*	*18.19*	*0.04613*	*3.45*	*0.19*	*17.646*	*17.86*	*290.7*	*10.3*	*313*	*64*	*479*	*197*
0306—9T2	432	3990	1.8	0.14059	11.89	0.01894	2.76	0.23	18.571	11.57	120.9	3.4	134	17	365	130
0306—10T	997	1557	7.9	0.10613	17.85	0.01810	1.96	0.11	23.513	17.75	115.6	2.3	102	19	−195	222
0306—12T	475	4107	4.9	0.14175	8.25	0.01793	3.58	0.43	17.442	7.44	114.6	4.1	135	12	504	82
0306—13T	88	1123	3.1	0.17018	54.74	0.01948	6.46	0.12	15.781	54.36	124.4	8.1	160	90	721	577
0306—14C	99	844	1.5	0.20605	26.25	0.01928	7.37	0.28	12.900	25.19	123.1	9.1	190	53	1135	251
0306—14T	943	3211	7.1	0.12005	11.99	0.01722	2.57	0.21	19.779	11.71	110.1	2.9	115	15	221	136
0306—15T	298	1725	0.9	0.12927	19.51	0.01747	1.97	0.10	18.631	19.41	111.6	2.2	123	25	357	219
0306—16T	*443*	*12,471*	*2.3*	*0.31605*	*10.18*	*0.04144*	*4.24*	*0.42*	*18.080*	*9.26*	*261.8*	*11.3*	*279*	*32*	*425*	*103*
0306—16C	*59*	*2088*	*1.6*	*0.37313*	*35.31*	*0.03991*	*3.22*	*0.09*	*14.749*	*35.16*	*252.3*	*8.3*	*322*	*126*	*863*	*365*
0306—17C	*110*	*2054*	*1.6*	*0.16307*	*25.01*	*0.02232*	*6.64*	*0.27*	*18.875*	*24.11*	*142.3*	*9.5*	*153*	*41*	*328*	*274*
0306—18C	*52*	*1584*	*1.2*	*0.17922*	*37.98*	*0.02407*	*6.66*	*0.18*	*18.519*	*37.39*	*153.3*	*10.3*	*167*	*67*	*371*	*421*
0309—1T	182	1601	2.3	0.14091	43.83	0.01895	5.73	0.13	18.546	43.46	121.0	7.0	134	61	368	490
0309—1C	37	1390	1.8	0.22280	30.61	0.02934	9.40	0.31	18.154	29.13	186.4	17.7	204	67	416	325
0309—2T	221	1643	1.4	0.14810	21.39	0.01920	4.05	0.19	17.877	21.00	122.6	5.0	140	32	450	233
0309—2T2	237	1707	2.0	0.14546	20.95	0.01881	3.00	0.14	17.825	20.73	120.1	3.6	138	30	456	230
0309—2C	58	616	0.7	0.17613	56.37	0.02638	5.40	0.10	20.647	56.11	167.8	9.2	165	96	120	661
0309—3T	233	1825	1.9	0.14647	18.99	0.02000	2.72	0.14	18.827	18.79	127.7	3.5	139	28	334	213
0309—3C	94	613	1.1	0.24051	28.62	0.02693	5.66	0.20	15.437	28.06	171.3	9.8	219	68	767	295
0309—4T	173	1112	1.6	0.13303	33.13	0.01861	2.92	0.09	19.293	33.00	118.9	3.5	127	44	278	378
0309—4C	292	1589	2.2	0.14856	24.30	0.01923	2.77	0.11	17.847	24.14	122.8	3.4	141	36	454	268
0309—5T	104	1731	2.0	0.15353	34.35	0.02083	4.11	0.12	18.711	34.10	132.9	5.5	145	52	348	386
0309—5C	29	1238	3.5	0.17859	23.64	0.02840	4.26	0.18	21.925	23.25	180.5	7.8	167	42	−23	281
0309—5C2	36	1321	2.9	0.15306	32.73	0.02660	4.59	0.14	23.964	32.41	169.3	7.9	145	50	−243	409
0309—6T	286	2505	1.7	0.13547	16.58	0.01922	1.94	0.12	19.562	16.46	122.7	2.4	129	23	246	190
0309—6T2	251	1800	1.4	0.11983	25.08	0.01896	5.12	0.20	21.811	24.55	121.1	6.3	115	30	−10	297
0309—6C	*129*	*1007*	*1.6*	*0.15502*	*39.73*	*0.02369*	*2.89*	*0.07*	*21.073*	*39.63*	*151.0*	*4.4*	*146*	*61*	*72*	*471*
0309—7T	133	1005	1.7	0.18016	28.05	0.02100	5.21	0.19	16.075	27.57	134.0	7.1	168	50	681	294
0309—7T2	233	4232	1.2	0.15461	15.80	0.01908	3.78	0.24	17.016	15.34	121.8	4.6	146	24	558	167
0309—7C	36	1475	1.1	0.16055	48.18	0.02586	5.56	0.12	22.206	47.86	164.6	9.3	151	76	−54	583

(continued on next page)

Table 2 (*continued*)

						Isotopic ratios					Apparent ages (Ma)					
Sample–grain	U (ppm)	$^{206}Pb/^{204}Pb$	U/Th	$^{207}Pb^*/^{235}U$	± (%)	$^{206}Pb^*/^{238}U$	± (%)	Error corr.	$^{206}Pb/^{207}Pb$	± (%)	$^{206}Pb^*/^{238}U$	± (Ma)	$^{207}Pb^*/^{235}U$	± (Ma)	$^{206}Pb^*/^{207}Pb^*$	± (Ma)
0309—8T	95	976	3.3	0.11405	40.25	0.01900	5.16	0.13	22.970	39.92	121.3	6.3	110	46	−137	494
0309—8T2	125	1250	1.9	0.18058	46.59	0.01961	4.07	0.09	14.974	46.41	125.2	5.1	169	82	831	484
0309—9T	250	1391	1.6	0.11688	28.17	0.01951	3.20	0.11	23.022	27.99	124.6	4.0	112	33	−142	347
0309—9T2	239	1205	1.8	0.17214	17.14	0.01930	2.03	0.12	15.460	17.02	123.2	2.5	161	30	764	179
0309—9C	60	504	2.0	0.18443	42.97	0.02641	6.81	0.16	19.746	42.42	168.1	11.6	172	77	225	490
0309—11T	181	1455	2.8	0.11859	22.64	0.01989	1.33	0.06	23.123	22.60	127.0	1.7	114	27	−153	281
0309—12T	199	927	2.4	0.12930	32.56	0.02007	2.75	0.08	21.398	32.45	128.1	3.6	123	42	36	388
0309—12T2	85	1790	6.5	0.14615	60.92	0.02030	6.43	0.11	19.155	60.58	129.6	8.4	139	87	294	691
0309—12T3	125	1766	2.6	0.15797	26.11	0.01957	6.02	0.23	17.083	25.40	124.9	7.6	149	41	550	277
0309—12T4	168	1199	2.3	0.14190	31.91	0.01917	4.01	0.13	18.622	31.66	122.4	5.0	135	45	358	357
0309—12C	839	4996	0.4	0.17858	11.09	0.02684	3.73	0.34	20.722	10.44	170.7	6.5	167	20	112	123
0309—13T	135	826	2.1	0.09282	41.80	0.01998	3.25	0.08	29.672	41.68	127.5	4.2	90	39	−815	593
0309—13C	15	1234	0.9	0.21125	42.70	0.02791	4.79	0.11	18.218	42.43	177.5	8.6	195	88	408	475
0309—14T	156	1197	2.8	0.13329	35.60	0.01995	2.83	0.08	20.637	35.48	127.3	3.6	127	47	122	418
0309—14C	68	880	1.2	0.14218	36.88	0.02661	4.63	0.13	25.808	36.58	169.3	7.9	135	52	−434	480
0309—14T2	220	1649	1.5	0.14315	18.72	0.01832	2.99	0.16	17.649	18.48	117.1	3.5	136	27	478	204

Analyses in normal black text were used in calculating weighted mean ages. These ages cluster into two groups, an older group and a younger group. Analyses in italics are not used in calculating ages. Analyses that end in T are from the tips of grains, analyses ending in C are from cores. All errors are reported at the 1σ level and incorporate only uncertainties from measurement of isotopic ratios. U concentration and U/Th have uncertainty of ~25%. Decay constants are as follows: $^{235}U = 9.8485 \times 10^{-10}$, $^{238}U = 1.55125 \times 10^{-10}$, $^{238}U/^{235}U = 137.88$. Isotope ratios are corrected for Pb/U fractionation by comparison with standard zircon with an age of 564 ± 4 Ma. Initial Pb composition interpreted from Stacey and Kramers (1975), with uncertainties of 1.0 for $^{206}Pb/^{204}Pb$ and 0.3 for $^{207}Pb/^{204}Pb$.

tance in the field and Alex Pullen assisted with the U–Pb geochronologic procedures.

Appendix A. U–Pb analytical methods

Zircons from three samples were analyzed with a Micromass Isoprobe multicollector ICPMS equipped with 9 Faraday collectors, an axial Daly detector, and 4 ion-counting channels. The Isoprobe is equipped with a New Wave DUV 193 laser ablation system with an emission wavelength of 193 nm. The analyses were conducted on 25–50 μm spots with an output energy of ~32 mJ and a repetition rate of 8 Hz. Each analysis consisted of one 30-second integration on the backgrounds (on peaks with no laser firing) and twenty one-second integrations on peaks with the laser firing. The depth of each ablation pit is ~20 μm . The collector configuration allows simultaneous measurement of ^{204}Pb in a secondary electron multiplier while ^{206}Pb, ^{207}Pb, ^{208}Pb, ^{232}Th, and ^{238}U are measured with Faraday detectors. All analyses were conducted in static mode.

Correction for common Pb was done by measuring $^{206}Pb/^{204}Pb$, with the composition of common Pb from Stacey and Kramers (1975) and uncertainties of 1.0 for $^{206}Pb/^{204}Pb$ and 0.3 for $^{207}Pb/^{204}Pb$. Fractionation of $^{206}Pb/^{238}U$ and $^{206}Pb/^{207}Pb$ during ablation was monitored by analyzing fragments of a large concordant zircon crystal that has a known (ID-TIMS) age of 564 ± 4 Ma (2σ) (G.E. Gehrels, unpublished data). Typically this reference zircon was analyzed once for every four unknowns. The uncertainty arising from this calibration correction contributed ~2% systematic error to the $^{206}Pb/^{238}U$ and $^{206}Pb/^{207}Pb$ ages (2σ level). The uncertainty from decay constants and common Pb composition yielded an additional ~1% systematic error to each analysis.

The reported ages are based primarily on $^{206}Pb/^{238}U$ ratios because the errors of the $^{207}Pb/^{235}U$ and $^{206}Pb/^{207}Pb$ ratios are significantly greater (Table 2). This is due in large part to the low intensity (commonly ~1 mV) of the ^{207}Pb signal from these young grains. For each of the samples, the age data are plotted on a Pb/U concordia diagram, and the critical $^{206}Pb/^{238}U$ ages are shown on a separate age plot (using the plotting program of Ludwig, 2001). The final age calculations are based on the weighted mean of the cluster of $^{206}Pb/^{238}U$ ages, with the error

expressed both as the uncertainty of this mean and as the error of the age. The age error is based on the quadratic sum of the weighted mean error and the systematic error. Both are expressed at the 2σ level.

References

Allibone, A.H., Tulloch, A.J., 1997. Metasedimentary, granitoid and gabbroic rocks from central Stewart Island, New Zealand. New Zealand Journal of Geology and Geophysics 40, 53–68.

Blattner, P., 1976. Replacement of hornblende by garnet in granulite facies assemblages near Milford Sound, New Zealand. Contributions to Mineralogy and Petrology 55, 181–190.

Blattner, P., 1978. Geology of crystalline basement between Milford Sound and the Hollyford Valley, New Zealand. New Zealand Journal of Geology and Geophysics 21, 33–47.

Blattner, P., 1991. The North Fiordland transcurrent convergence. New Zealand Journal of Geology and Geophysics 34, 535–542.

Blattner, P., Graham, I.G., 2000. New Zealand's Darran Complex and Mackay Intrusives — Rb/Sr whole-rock isochrons in the Median Tectonic Zone. American Journal of Science 300, 603–629.

Bradshaw, J.D., 1989a. Cretaceous geotectonic patterns in the New Zealand region. Tectonics 8 (4), 803–820.

Bradshaw, J.Y., 1989b. Origin and metamorphic history of an early cretaceous polybaric granulite terrain, Fiordland, southwest New Zealand. Contributions to Mineralogy and Petrology 103, 346–360.

Bradshaw, J.Y., 1990. Geology of crystalline rocks of northern Fiordland: details of the granulite facies Western Fiordland orthogneiss and associated rock units. New Zealand Journal of Geology and Geophysics 33, 465–484.

Bradshaw, J.D., 1993. A review of the median tectonic zone: terrane boundaries and terrane amalgamation near the median tectonic line. New Zealand Journal of Geology and Geophysics 36, 117–125.

Bradshaw, J.Y., Kimbrough, D.L., 1989. Comment: age constraints on metamorphism and the development of a metamorphic core complex in Fiordland, southern New Zealand. Geology 17, 380–381.

Brown, E.H., 1996. High-pressure metamorphism caused by magma loading in Fiordland, New Zealand. Journal of Metamorphic Geology 14, 441–452.

Cembrano, J., Lavenu, A., Reynolds, P., Arancibia, J., López, G., Sanhueza, A., 2002. Late Cenozoic transpressional ductile deformation north of the Nazca–South America–Antarctica triple junction. Tectonophysics 354, 289–314.

Clarke, G.L., Klepeis, K.A., Daczko, N.R., 2000. Cretaceous high-P granulites at Milford Sound, New Zealand: metamorphic history and emplacement in a convergent margin setting. Journal of Metamorphic Geology 18, 359–374.

Clarke, G.L., Daczko, N.R., Klepeis, K.A., Rushmer, T., 2005. Roles for fluid and/or melt advection in forming high-P mafic migmatites, Fiordland, New Zealand. Journal of Metamorphic Geology 23, 557–567.

Claypool, A., Klepeis, K., Dockrill, B., Clarke, G., Zwingmann, H., Tulloch, A., 2002. Structure and kinematics of oblique continental convergence in Northern Fiordland, New Zealand. Tectonophysics 359, 329–358.

Coke, C., Dias, R., Ribeiro, A., 2003. Rheologically induced structural anomalies in transpressive regimes. Journal of Structural Geology 25 (3), 409–420.

Czeck, D.M., Hudleston, P.J., 2003. Testing models for obliquely plunging lineations in transpression: a natural example and theoretical discussion. Journal of Structural Geology 25, 959–982.

Czeck, D.M., Hudleston, P.J., 2004. Physical experiments of vertical transpression with localized nonvertical extrusion. Journal of Structural Geology 26, 573–581.

Daczko, N., Clarke, G.L., Klepeis, K.A., 2001a. The transformation of two-pyroxene-amphibole granulite to garnet granulite; simultaneous melting and fracturing of the lower crust. Fiordland, New Zealand. Journal of Metamorphic Geology 19, 547–560.

Daczko, N.R., Klepeis, K.A., Clarke, G.L., 2001b. Evidence of Early Cretaceous collisional-style orogenesis in northern Fiordland, New Zealand and its effects on the evolution of the lower crust. Journal of Structural Geology 23, 693–713.

Daczko, N.R., Clarke, G.L., Klepeis, K.A., 2002a. Kyanite–paragonite-bearing assemblages, northern Fiordland, New Zealand: rapid cooling of the lower crustal root to a cretaceous magmatic arc. Journal of Metamorphic Geology 20, 887–902.

Daczko, N.R., Clarke, G.L., Klepeis, K.A., 2002b. Successive hydration and dehydration of high-P mafic granofels involving clinopyroxene–kyanite symplectites, Mt Daniel Fiordland New Zealand. Journal of Metamorphic Geology 20, 669–682.

Daczko, N.R., Klepeis, K.A., Clarke, G.L., 2002c. Thermomechanical evolution of the crust during convergence and deep crustal pluton emplacement in the Western Province of Fiordland, New Zealand. Tectonics 21 (4), 1–18.

Dewey, J.F., Holdsworth, R.E., Strachan, R.A., 1998. Transpression and transtension zones. In: Holdsworth, R.E., Strachan, R.A., Dewey, J.F. (Eds.), Continental Transpressional and Transtensional Tectonics, Geological Society Special Publications, vol. 135, pp. 1–14.

Flowers, R.M., Bowring, S.A., Tulloch, A.J., Klepeis, K.A., 2005. Tempo of burial and exhumation within the deep roots of a magmatic arc, Fiordland, New Zealand. Geology 33 (1), 17–20.

Gibson, G.M., Ireland, T.R., 1995. Granulite formation during continental extension in Fiordland. Nature 375, 479–482.

Hollis, J.A., Clarke, G.L., Klepeis, K.A., Daczko, D.A., Ireland, T.R., 2003. Geochronology and Geochemistry of high-pressure granulites of the Arthur River Complex, Fiordland, New Zealand: cretaceous magmatism and metamorphism on the palaeo-pacific margin. Journal of Metamorphic Geology 21, 299–313.

Hollis, J.A., Clarke, G.L., Klepeis, K.A., Daczko, N.R., Ireland, T.R., 2004. The regional significance of Cretaceous magmatism and metamorphism in Fiordland, New Zealand, from U–Pb zircon geochronology. Journal of Metamorphic Geology 22, 607–627.

Ji, S., Mainprice, D., 1990. Recrystallization and fabric development in plagioclase. Journal of Geology 98, 65–79.

Jiang, D., Lin, S., Williams, P.F., 2001. Deformation path in high-strain zones, with reference to slip partitioning in transpressional plate-boundary regions. Journal of Structural Geology 23, 991–1005.

Jones, R.R., Holdsworth, R.E., Clegg, P., McCaffrey, K., Tavarnelli, E., 2004. Inclined transpression. Journal of Structural Geology 26, 1531–1548.

Kimbrough, D.L., Tulloch, A.J., Geary, E., Coombs, D.S., Landis, C.A., 1993. Isotope ages from the Nelson region of South Island, New Zealand: structure and definition of the median tectonic zone. Tectonophysics 225, 433–448.

Kimbrough, D.L., Tulloch, A.J., Coombs, D.S., Landis, C.A., Johnston, M.R., Mattinson, J.M., 1994. Uranium–lead zircon ages from the median tectonic zone, New Zealand. New Zealand Journal of Geology and Geophysics 37, 393–419.

Klepeis, K.A., Clarke, G.L., 2004. Evolution of an exposed lower crustal attachment zone in Fiordland, New Zealand. In: Grocott, J., McCaffrey, K., Taylor, G., Tikoff, B. (Eds.), Vertical Coupling and Decoupling in the Lithosphere, Geological Society of London, Special Publication, vol. 227, pp. 197–229.

Klepeis, K.A., Crawford, M.L., 1999. High temperature, arc-parallel normal faulting at the roots of an obliquely convergent orogen. Geology 27, 7–10.

Klepeis, K.A., Daczko, D.R., Clarke, G.L., 1999. Kinematic vorticity and tectonic significance of superposed mylonites in a major lower crustal shear zone, northern Fiordland, New Zealand. Journal of Structural Geology 21, 1385–1405.

Klepeis, K.A., Clarke, G.L., Gehrels, G., Vervoort, J., 2004. Processes controlling vertical coupling and decoupling between the upper and lower crust of orogens: results from Fiordland, New Zealand. Journal of Structural Geology 26 (4), 765–791.

Koons, P.O., 1978. Aspects of the geology of the southern Darran Mountains. New Zealand Geological Survey Report G 26.

Kruse, R., Stunitz, H., 1999. Deformation mechanisms and phase distribution in mafic high-temperature mylonites from the Jotun Nappe, southern Norway. Tectonophysics 303, 223–249.

Lin, S., Jiang, D., William, P.F., 1998. Transpression (or transtension) zones of triclinic symmetry: natural example and theoretical modelling. In: Holdsworth, R.E., Strachan, R.A., Dewey, J.F. (Eds.), In Continental Transpressional and Transtensional Tectonics, Geological Society of London, Special Publication, vol. 135, pp. 41–75.

Ludwig, K.J., 2001. Isoplot/Ex (rev. 2.49): Berkeley Geochronology Center Special Publication No. 1a. 56 pp.

Mattinson, J.L., Kimbrough, D.L., Bradshaw, J.Y., 1986. Western Fiordland orthogneiss: early cretaceous arc magmatism and granulite facies metamorphism, New Zealand. Contributions to Mineralogy and Petrology 92, 383–392.

McCaffrey, R., 1992. Oblique plate convergence, slip vectors, and forearc deformation. Journal of Geophysical Research 97, 8905–8915.

Mortimer, N., Gans, P.B., Calvert, A., Walker, N., 1999a. Geology and thermochronometry of the east edge of the median batholith (Median Tectonic Zone); a new perspective on permian to cretaceous crustal growth of New Zealand. The Island Arc 8, 404–425.

Mortimer, N., Tulloch, A.J., Spark, R., Walker, N., Ladley, E., Kimbrough, D.L., Allibone, A.H., 1999b. Overview of the median batholith, New Zealand: a new interpretation of the geology of the median tectonic zone and adjacent rocks. Journal of African Earth Sciences 29, 257–268.

Muir, R.J., Weaver, S.D., Bradshaw, J.D., Eby, G.N., Evans, J.A., 1995. The cretaceous separation point batholith, New Zealand: granitoid magmas formed by melting of a mafic lithosphere. Journal of the Geological Society (London) 152 (4), 689–701.

Muir, R.J., Ireland, T.R., Weaver, S.D., Bradshaw, J.D., Evans, J.A., Eby, G.N., Shelly, D., 1998. Geochronology and geochemistry of a mesozoic magmatic arc system, Fiordland, New Zealand. Journal of the Geological Society (London) 155 (6), 1037–1053.

Nathan, S., Thurlow, C., Warnes, P., Zucchetto, R., 2000. Geochronology database for New Zealand rocks (2nd edition): 1961–1999. Institute of Geological and Nuclear Sciences Report 2000/11, pp. 1–51.

Norris, R.J., Cooper, A.F., 1995. Origin of small-scale segmentation and transpressional thrusting along the Alpine fault, New Zealand. Geological Society of America Bulletin 107, 231–240.

Oliver, G.J.H., 1990. An exposed cross-section of continental crust, doubtful sound, Fiordland, New Zealand; geophysical and geological setting. In: Salisbury, M.H., Fountain, D.M. (Eds.), Exposed Cross Sections of the Continental Crust. Kluwer Academic Publishers, pp. 43–69.

Olsen, S.V., Kohlstedt, D.L., 1985. Natural deformation and recrystallization of some intermediate plagioclase feldspars. Tectonophysics 111, 107–131.

Passchier, C.W., Trouw, R.A.J., 1996. Microtectonics. Springer Verlag, Berlin, p. 106.

Pryer, L.L., 1993. Microstructures in feldspars from a major crustal thrust zone, the Grenville Front, Ontario, Canada. Journal of Structural Geology 15, 21–36.

Rosenberg, C.L., Stunitz, H., 2003. Deformation and recrystallization of plagioclase along a temperature gradient: an example from the Bergell tonalite. Journal of Structural Geology 25, 389–408.

Rubatto, D., Williams, I.S., Buck, I.S., 2001. Zircon and monazite response to prograde metamorphism in the Reynolds range, central Australia. Contributions to Mineralogy and Petrology 140, 458–468.

Saint Blanquat, M., Tikoff, B., Teyssier, C., Vigneresse, J.L., 1998. Transpressional kinematics and magmatic arcs. In: Holdsworth, R.E., Strachan, R.A., Dewey, J.F. (Eds.), Continental Transpressional and Transtensional Tectonics, Geological Society of London, Special Publications, vol. 135, pp. 327–340.

Stacey, J.S., Kramers, J.D., 1975. Approximation of terrestrial lead isotope evolution by a two-stage model. Earth and Planetary Science Letters 26, 207–221.

Tavarnelli, E., Holdsworth, R.E., Clegg, P., Jones, R.R., McCaffrey, K.J.W., 2004. The anatomy and evolution of a transpressional imbricate zone, Southern Uplands, Scotland. Journal of Structural Geology 26 (8), 1341–1360.

Teyssier, C., Tikoff, B., 1998. Strike-slip partitioned transpression of the San Andreas fault system; a lithospheric scale approach. In: Holdsworth, R.E., Strachan, R.A., Dewey, J.F. (Eds.), Continental Transpressional and Transtensional Tectonics, Geological Society Special Publications, vol. 135, pp. 143–158.

Tikoff, B., Teyssier, C., 1994. Structures and tectonics at different lithospheric levels: a selection of papers presented at the international conference. Journal of Structural Geology 16 (11), 1575–1588.

Tullis, J., Yund, R.A., 1985. Dynamic recrystallization of feldspar: a mechanism for ductile shear zone formation. Geology 13, 238–241.

Tulloch, A.J., Kimbrough, D.L., 2003. Paired plutonic belts in convergent margins and the development of high Sr/Y magmatism: peninsular ranges batholith of Baja-California and Median batholith of New Zealand. In: Johnson, S.E., Paterson, S.R., Fletcher, J.M., Girth, G.H., Kimbrough, D.L., Martin-Barajas, A. (Eds.), Tectonic Evolution of Northwestern Mexico and the Southwestern USA: Boulder, Colorado, Geological Society of America, Special Paper, vol. 374, pp. 275–295.

Tulloch, A.J., Ireland, T.R., Walker, N.W., Kimbrough, D.L., 2000. U–Pb zircon ages from the Milford Orthogneiss, Milford Sound, Northern Fiordland: paleozoic igneous emplacement and early cretaceous metamorphism. Institute for Geological and Nuclear Sciences Report 6 (17).

Turnbull, I.M., 2000. Geology of the Wakatipu area. Institute of Geological and Nuclear Sciences geologic map 18, 1 sheet +72, Lower Hutt, New Zealand, scale 1:25 0000.

Wandres, A.M., Weaver, S.D., Shelley, D., Bradshaw, J.D., 1998. Change from calc–alkaline to adakitic magmatism recorded in the early cretaceous Darran Complex, Fiordland, New Zealand. New Zealand Journal of Geology and Geophysics 41, 1–14.

Williams, I.S., 2001. Response of detrital zircon and monazite, and their U–Pb isotopic systems, to regional metamorphism and host-rock partial melting, Cooma complex, southeastern Australia. Australian Journal of Earth Sciences 48, 557–580.

Wood, B.L., 1962. New Zealand Geological Survey Map 1:25 0000, Sheet 22, Wakatipu, First Edition.

Wood, B.L., 1972. Metamorphosed ultramafites and associated formations near Milford Sound, New Zealand. New Zealand Journal of Geology and Geophysics 15, 88–127.